

The Galaxy Correlation Function in the CNOC2 Redshift Survey: Dependence on Color, Luminosity and Redshift

C. W. Shepherd¹, R. G. Carlberg^{1,2}, H. K. C. Yee^{1,2}, S. L. Morris^{2,3}, H. Lin^{2,4,5}, M. Sawicki^{2,6}, P. B. Hall^{2,7}, and D. R. Patton^{1,2}

ABSTRACT

We examine how the spatial correlation function of galaxies from the CNOC2 Field Galaxy Redshift Survey depends on galaxy color, luminosity and redshift. The projected correlation function w_p is determined for volume-limited samples of objects with $0.12 \leq z < 0.51$ and evolution-compensated R_C -band absolute magnitudes $M_R^0 < -20$, over the comoving projected separation range $0.04 h^{-1} \text{Mpc} < r_p < 10 h^{-1} \text{Mpc}$. Our sample consists of 2937 galaxies which are classified as being either early- or late-type objects according to their spectral energy distribution (SED), determined from $UBVR_CI_C$ photometry. For simplicity, galaxy SEDs are classified independently of redshift: our classification scheme therefore does not take into account the colour evolution of galaxies.

Objects with SEDs corresponding to early-type galaxies are found to be more strongly clustered by a factor of ~ 3 , and to have a steeper correlation function, than those with late-type SEDs. Modeling the spatial correlation function, as a function of comoving separation r , as $\xi(r) = (r/r_0)^{-\gamma}$, we find $r_0 = 5.45 \pm 0.28 h^{-1} \text{Mpc}$ and $\gamma = 1.91 \pm 0.06$ for early-type objects, and $r_0 = 3.95 \pm 0.12 h^{-1} \text{Mpc}$ and $\gamma = 1.59 \pm 0.08$ for late-type objects (for $\Omega_M = 0.2$, $\Omega_\Lambda = 0$). While changing the cutoff between early-

¹Department of Astronomy and Astrophysics, University of Toronto, Toronto, Ontario, M5S 3H8, Canada. Email: carlberg, hyee, patton, and shepherd@astro.utoronto.ca.

²Visiting Astronomer, Canada-France-Hawaii Telescope, which is operated by the National Research Council of Canada, Le Centre National de Recherche Scientifique, and the University of Hawaii.

³Department of Physics, University of Durham, Rochester Building, Science Laboratories, South Road, Durham, DH1 3LE, England. Email: simon.morris@durham.ac.uk.

⁴Steward Observatory, University of Arizona, Tucson, AZ, 85721. Email: hlin@as.arizona.edu.

⁵Hubble Fellow.

⁶Department of Physics, California Institute of Technology, Mail Code 320-47, Pasadena, CA, 91125. Email: sawicki@pirx.caltech.edu.

⁷Princeton University Observatory and Pontificia Universidad Católica de Chile, Departamento de Astronomía y Astrofísica, Facultad de Física, Casilla 306, Santiago 22, Chile. E-mail: phall@astro.puc.cl

and late-type SEDs does affect the correlation amplitudes of the two samples, the ratio of the amplitudes remains constant to within 10%.

The redshift dependence of the correlation function also depends on SED type. Modeling the redshift dependence of the comoving correlation amplitude r_0^γ as $r_0^\gamma(z) \propto (1+z)^{\gamma-3-\epsilon}$, we find that early-type objects have $\epsilon = -3.9 \pm 1.0$, and late-type objects have $\epsilon = -7.7 \pm 1.3$. Both classes of objects therefore have clustering amplitudes, measured in comoving coordinates, which appear to decrease rapidly with cosmic time. The excess clustering of galaxies with early-type SEDs, relative to late-type objects, is present at all redshifts in our sample. In contrast to the early- and late-type SED samples, the combined sample undergoes little apparent evolution, with $\epsilon = -2.1 \pm 1.3$, consistent with earlier results.

The apparent increase with redshift of the clustering amplitude in the early- and late-type samples is almost certainly caused by evolution of the galaxies themselves, rather than by evolution of the correlation function. If galaxy SEDs have evolved significantly since $z \sim 0.5$, then our method of classifying SEDs may cause us to overestimate the true evolution of the clustering amplitude for the unevolved counterparts to our early- and late-type samples. However, if color evolution is to explain the apparent clustering evolution, the color evolution experienced by a galaxy must be correlated with the galaxy correlation function.

We also investigate the luminosity dependence of the correlation function for volume-limited samples with $0.12 \leq z < 0.40$ and $M_R^0 < -19.25$. We detect a weak luminosity dependence of the correlation amplitude for galaxies with early-type SEDs, $d \log \xi / dM_R^0 = -0.35 \pm 0.17$, but no significant dependence for late-type objects, $d \log \xi / dM_R^0 = 0.02 \pm 0.16$.

Subject headings: galaxies: clustering — galaxies: evolution — large-scale structure of universe

1. Introduction

At low redshift, the clustering of galaxies is observed to depend both on luminosity and on morphological type. This behavior is expected if galaxies are biased tracers of the mass distribution in the universe, since the amount of biasing for a particular population depends on that population’s mass and formation mechanism. That clustering depends on galaxy morphology is generally accepted (e.g., Loveday et al. 1995; Hermit et al. 1996; Willmer, Da Costa, & Pellegrini 1998). Early-type galaxies are found to be more strongly clustered than late-type objects; estimates of the ratio of correlation function amplitudes for the two types range from ~ 1.5 to ~ 5 . The luminosity dependence of the correlation function is more contentious, although results from most recent redshift surveys (Loveday et al. 1995; Hermit et al. 1996; Lin et al. 1996; Willmer et al. 1998; Guzzo et al. 2000) do indicate that high-luminosity objects are more strongly clustered than

low-luminosity galaxies, with estimates of $d \log \xi / dM$ ranging from 0.1 to $\gtrsim 1$.

The luminosity and morphology dependence of the correlation function may vary with redshift, however, as the evolution of bias may be different for objects of different masses (Mo & White 1996; Matarrese et al. 1997; Baugh et al. 1999). Luminosity- and type-dependent evolution is also seen in semi-analytic models (Baugh et al. 1999; Kauffmann et al. 1999). The emerging picture of slowly- or non-evolving galaxy clustering (Small et al. 1999; Carlberg et al. 2000b; Hogg, Cohen, & Blandford 2000) may therefore hide some important details. Obtaining an empirical estimate of the evolution of the correlation function, either as a function of luminosity, or of galaxy type, is extremely challenging, however, due to the difficulty of defining a non-evolving sample of galaxies.

We present here correlation function measurements for 2937 galaxies from the Canadian Network for Observational Cosmology Field Galaxy Redshift Survey (CNOC2; Yee et al. 2000). Attempts to measure the correlation function for different types of objects in deep-redshift surveys have so far employed samples defined by a galaxy’s color as determined by a single color index (Le Fèvre et al. 1996; Carlberg et al. 1998) or on the strength of the [O II] line (Cole et al. 1994; Small et al. 1999). Rather than rely on a single color index or line strength, we classify galaxies according to their spectral energy distributions (SEDs), determined from $UBVR_CI_C$ photometry. As opposed to most morphological classification systems, our SED-based classification scheme has the additional advantage of being completely quantitative. The large number of objects in the survey allows us to investigate not only the dependence of the correlation function on color, luminosity and redshift, but also the joint color-luminosity and color-redshift dependences.

Our classification scheme does not account for the evolution of galaxy SEDs. Therefore, both SED evolution and true evolution of the galaxy correlation function will contribute to the apparent redshift dependence of the correlation function in our SED-selected samples. Despite this ambiguity, useful constraints on the evolution of the correlation function may be obtained using this technique, independently of any particular model for the evolution of galaxy SEDs.

This paper is organized as follows: In §2, we describe the data used in our analysis. Section 3 describes our technique for estimating the correlation function from these data. In §4, we describe how the correlation function depends on galaxy color, redshift and luminosity; these results are discussed, and compared to those from other works, in §5. Throughout this paper, we take $\Omega_M = 0.2$, $\Omega_\Lambda = 0$, and $H_0 = 100h \text{ km s}^{-1} \text{ Mpc}^{-1}$; absolute magnitudes are expressed using $h = 1$. As the estimated correlation function depends on Ω_M and Ω_Λ through the angular separation-redshift relation, changing these parameters would result in a different estimate of the evolution of the correlation function. However, Carlberg et al. (2000b), using a sample of data from the CNOC2 survey similar to that used here, find that the correlation length changes by $\lesssim 7\%$ when different cosmological parameters are assumed. The variation of our results with cosmology is therefore likely to be small compared to the statistical uncertainties.

2. The CNOC2 Survey Data

The CNOC2 Field Galaxy Redshift Survey is described in detail by Yee et al. (2000; also see Yee, Ellingson, & Carlberg 1996). We summarize here only the relevant aspects of the survey.

The sample consists of over 5000 redshifts for objects with $R_C < 21.5$. The rms velocity errors, determined from redundant observations, are $\sim 100 \text{ km s}^{-1}$. The data were obtained at the Canada-France-Hawaii Telescope (CFHT) using the CFHT Multi-Object Spectrograph (MOS). The survey covers four widely separated areas (“patches”) on the sky: 0223+00, 0920+37, 1447+09, 2148-05 (labeled by RA and Dec). Each patch is roughly L-shaped, and comprises between 17 and 19 MOS fields, each of which is approximately 9 arc-minutes by 8 arc-minutes in size. The data used here are from the most recent version of the CNOC2 catalog, a portion of which is available electronically: see Yee et al. (2000) for details.

As discussed in §1, galaxy clustering is known to depend on luminosity, with low-luminosity galaxies being less strongly correlated than those with high luminosity. This effect will cause the correlation function estimated from a magnitude-limited sample to exhibit apparent redshift evolution, in addition to any evolution caused by true changes of clustering, as only brighter objects will be included in the sample at higher redshifts. To avoid this effect, we consider only volume-limited samples in this analysis.

A further complication is that galaxies undergo substantial luminosity evolution over the redshift range of the sample. Lin et al. (1999) find that the characteristic magnitude, M_* , of the luminosity function for the CNOC2 sample evolves as $M_*(z) = M_*(0) - Qz$, where the R_C -band evolution parameter $Q = 1.51 \pm 0.53$ for objects with SED number s (defined in §2.1) in the range $-0.5 \leq s < 0.5$, 1.11 ± 0.78 for $0.5 \leq s < 1.5$, and 0.22 ± 0.76 for $1.5 \leq s < 3.5$. Therefore, to sample the same population of objects at different redshifts, we select galaxies based on their evolution-compensated R_C -band absolute magnitudes $M_R^0 = M_R + Qz$.

The selection function for our volume-limited samples differs from unity, due to varying observing conditions, non-uniform spatial sampling, MOS slit collision, etc. Yee et al. (2000) and Yee et al. (1996) have developed an accurate empirical estimate of these observational selections as a function of galaxy magnitude, color, position and redshift. While we do employ these estimates in our calculation of the correlation function, as discussed in §3, we find that ignoring the selection effects results only in small changes in the correlation function estimates, typically less than 5%.

2.1. Spectral Energy Distribution Classification

In addition to the large number of redshifts in the survey, the CNOC2 survey has the advantage of having $UBVR_CI_C$ photometry for nearly all objects. By comparing the observed colors to those predicted by redshifted template spectra, we classify each object as having either an early- or a late-type spectral energy distribution. This allows us to investigate the evolution of the clustering

of galaxies as a function of SED class, rather than simply as a function of any one particular color index or spectral feature.

The SED classification technique used here is the same as that used in Lin et al. (1999) to determine the luminosity function for the CNOC2 survey. We use template SEDs from Coleman, Wu, & Weedman (1980, hereafter CWW). We assign numerical values to the four CWW template SEDs as follows: template 0 is the Old Stellar Population (OSP) SED, taken to be the average of the M31 and M81 OSP SEDs. Templates 1, 2 and 3 are the CWW Sbc, Scd, and Im SED, respectively. To determine the SED number s of an object at a particular redshift, we compute the apparent magnitudes for each of these four template SEDs, in each of the five photometric bands, at the given redshift. We then add -0.05 mag to I_C for templates 0–2, in order to better match the observed $R_C - I_C$ colors of the data. We linearly interpolate the magnitudes between adjacent pairs of template SEDs, and linearly extrapolate the (0,1) pair to negative numbers and the (2,3) pair to numbers greater than 3. These interpolated magnitudes are then fit to the observed magnitudes (after correcting for Galactic reddening). The result of the least-squares fit is the best-fitting SED number s and rest-frame absolute magnitudes in each of the photometric bands.

Having obtained an SED number s for a galaxy, we classify it as having either an early- or a late-type SED: early-type objects are those with $s < 0.5$ (closest to the OSP SED); late-type objects have $s \geq 0.5$ (closest to Sbc, Scd or Im). Out of the 1993 objects in the survey which have $M_R^0 < -20$ and $0.12 \leq z < 0.51$, 720 are classified as having early-type SEDs, and 1273 as having late-type SEDs. Objects with $s < -0.5$ or $s \geq 3.5$ have SEDs which do not closely match any of the template SEDs and are therefore discarded; these objects constitute fewer than 2% of the data. Note that although our late-type sample corresponds to the combined intermediate plus late-type sample in Lin et al. (1999), we use the individual intermediate- and late-type luminosity functions to compute the evolution compensation Qz .

Our SED classification scheme does *not* account for evolution of galaxy color. An elliptical galaxy at redshift ~ 0.5 , for example, is expected to be somewhat bluer than one at redshift zero. If this color evolution is sufficiently strong, it is possible that a high-redshift object will have an SED which is a closer match to a CWW template SED of a later type than the true unevolved type of that object. Strong color evolution would therefore cause our late-type sample to contain progressively more E/S0 objects at higher redshifts, which could affect our determination of the redshift-dependence of the correlation function. This issue is discussed qualitatively in section §5, and will be addressed more thoroughly in a future paper.

3. Estimating the Correlation Function

We measure the spatial clustering of galaxies in the sample using the standard projected correlation function $w_p(r_p)$, defined as

$$w_p(r_p) = \int_{-\infty}^{\infty} \xi(r_p, r_z) dr_z \quad (1)$$

(Peebles 1980). Here, $\xi(r_p, r_z)$ is the two-point correlation function expressed as a function of separation perpendicular to (r_p) , and parallel to (r_z) , the line of sight to each pair of objects. The parallel component of the observed separation of a pair of objects, r_z , is the sum of their spatial separation and the relative peculiar velocity of the pair, projected on to the line-of-sight to the pair. As the integral in equation (1) is along the line-of-sight, w_p , unlike $\xi(r_p, r_z)$, is an estimate of the spatial clustering of galaxies, independent of their peculiar velocities. If the spatial two-point correlation function is described by a power-law, $\xi(r) = (r/r_0)^{-\gamma}$, then the projected correlation function will also be a power-law:

$$w_p(r_p) = C_\gamma r_0 (r_p/r_0)^{1-\gamma}, \quad (2)$$

where $C_\gamma = \sqrt{\pi} \Gamma((\gamma - 1)/2) / \Gamma(\gamma/2)$.

We estimate $\xi(r_p, r_z)$ as

$$\xi(r_p, r_z) = \frac{DD \cdot RR}{DR^2} - 1, \quad (3)$$

(Hamilton 1993), where DD is the weighted number of pairs of objects in the sample with separation (r_p, r_z) . The weights used for computing the pair counts are discussed in §3.1. The DR and RR pair counts in equation (3) are the weighted number of data-random and random-random pairs, respectively, where the random objects are drawn from a distribution which is unclustered, but otherwise the same as that of the data.

The random catalog is constructed so as to have the same redshift, color and magnitude distributions, and to be subject to the same selection effects, as the data. The luminosity function from Lin et al. (1999) determines the intrinsic joint distribution in redshift, magnitude and SED class; the distribution of SED numbers within an SED class is estimated directly from the data. A preliminary, unselected random catalog is generated from this distribution. Selection functions are then computed for each random object, by interpolating the selection functions for the data in color and magnitude. The final, selected random catalog is generated from the unselected catalog, the selection function for an object determining the probability that that object is included in the selected catalog.

Having obtained an estimate of $\xi(r_p, r_z)$ using equation (3), we integrate in the r_z direction, as in equation (1). We truncate the integral at $r_{z \text{ max}} = 25 h^{-1} \text{Mpc}$; no significant variation is seen in w_p as $r_{z \text{ max}}$ is varied between $15 h^{-1} \text{Mpc}$ and $100 h^{-1} \text{Mpc}$. The noise in w_p , however, increases substantially for $r_{z \text{ max}} > 25 h^{-1} \text{Mpc}$, as more physically unrelated pairs are added to the integral.

We estimate the uncertainty in the projected correlation function directly from the data, using the patch-to-patch variation in w_p . For a sample composed of N_{patch} independent, identical patches, with observed projected correlation functions $w_{p1}, \dots, w_{pN_{\text{patch}}}$, the variance in the mean,

$$\sigma_{w_p}^2 = \frac{1}{N_{\text{patch}}(N_{\text{patch}} - 1)} \sum_{i=1}^{N_{\text{patch}}} \left(w_{pi} - \frac{1}{N_{\text{patch}}} \sum_{j=1}^{N_{\text{patch}}} w_{pj} \right)^2, \quad (4)$$

is the best estimate of the square of the uncertainty in w_p , the projected correlation function computed from all N_{patch} patches combined.

Given estimates of w_p , and estimates of the uncertainty in w_p , the correlation function parameters r_0 and γ are determined from a least-squares fit of equation (2) to the data. The uncertainties in r_0 and γ are also estimated from the patch-to-patch variation, by fitting the data for each patch individually, to obtain r_{0i} and γ_i for each patch i . We then estimate the 1σ uncertainties in r_0 and γ for the full sample using equation (4), with w_p replaced by the appropriate quantity.

3.1. Pair Weights

The weight assigned to a pair of objects (i, j) with separation (r_p, r_z) in equation 3 is $w_{ij} = w_i w_j$, where

$$w_i = \frac{1}{1 + 2\pi\bar{n}\phi_i J_3(r_p, r_z)}. \quad (5)$$

Here, \bar{n} is the mean number density of objects in the sample, ϕ_i is the selection function for object i and $2\pi J_3(r_p, r_z)$ is the integral of the real-space correlation function over a cylinder of radius r_p and length $2r_z$. When computed with these weights, the resulting pair count DD will be the number of statistically independent pairs of objects with given r_p and r_z separations, so that our weighting scheme is analogous to the minimum-variance weighting suggested by Hamilton (1993) and Loveday et al. (1995) for the spatial correlation function $\xi(r)$.

Since equation (5) depends on the correlation function we are trying to estimate, via J_3 , we must use an iterative technique to determine the weights. We first compute $DD(< r_p, < r_z)$ and $DR(< r_p, < r_z)$, the number of data-data and data-random pairs, respectively, with separations $< r_p$ and $< r_z$, along with D and R , the number of data and random objects in the sample, respectively. These pair counts and object counts are computed with each object weighted by the inverse of its selection function. We then estimate the quantity $2\pi\bar{n}J_3(r_p, r_z)$ as the average number of objects in excess of random with separations $< r_p$ and $< r_z$ from a given object:

$$(2\pi\bar{n}J_3)_{\text{est}}(r_p, r_z) = \frac{DD(< r_p, < r_z)}{D} - \frac{DR(< r_p, < r_z)}{R}, \quad (6)$$

Finally, to estimate $\xi(r_p, r_z)$, we compute DD , DR , and RR in equation (3), using the pair weights defined by equation (5), with $2\pi\bar{n}J_3$ estimated as above.

In principle, we could refine the pair weights, by using the estimated correlation function and equation (2) to obtain an improved estimate of J_3 . However, J_3 computed in this fashion differs from that estimated using equation (6) by less than 10%. We consider this small inconsistency to be acceptable, as equation (5) is only an approximation to the minimum-variance weighting (Hamilton 1993), and equation (3) is an unbiased estimator of ξ , regardless of the weights used to compute the pair counts. Furthermore, there are no significant changes in the estimated correlations, and only marginally larger estimated uncertainties, if ξ is computed with each object weighted by the inverse of its selection function, or assigned a weight of unity. Since the weights defined by equation (5) lie somewhere between these two extreme cases, there is little point in further refinement of the estimate of J_3 .

4. Results

4.1. Color Dependence

To determine the color dependence of the correlation function, we consider three samples: the early-type SED sample (consisting of objects with $-0.5 \leq s < 0.5$), the late-type sample ($0.5 \leq s < 3.5$), and objects of all SED classes. All three samples have $0.12 \leq z < 0.51$ and $M_R^0 < -20$. These selection criteria yield volume-limited, evolution-compensated samples, in the sense that any object in the sample would still have $R_C = M_R + DM(z) + K(z) + Qz < 21.5$ if it were moved to any other redshift in the sample, where DM and K are the usual distance modulus and K-correction, respectively. We compute w_p as a function of projected comoving separation r_p for each SED sample, over the separation range $0.04 h^{-1}\text{Mpc} \leq r_p < 10 h^{-1}\text{Mpc}$. Fitting equation (2) to the data, we obtain r_0 and γ for each of these samples.

Our results are shown in Figure 1; the sample and fit parameters are given in Table 1. The correlation functions for all three samples are well-fit by the power-law model (2). There is, however, some slow variation of the data about the model, most evident in the late-type sample. This is expected, as the measured values of w_p at different separations are not independent, since the same galaxies contribute to pairs at all separations. Thus, if the observed w_p is greater (or less) than the universal value at some particular separation r_p , then it is likely that the w_p observed for adjacent separation bins will also be greater (less) than the universal value. Random scatter in the data will therefore have the visual appearance of a slow, non-random variation about the true correlation.

Given our limited range of separations, therefore, it is difficult to assess whether the model (2) is an adequate description of the data, or whether some other model, in which γ and r_0 vary with separation, is appropriate. However, even if the clustering is not well-described by a single power-law, the parameters r_0 and γ from that model may be interpreted as the correlation length and slope, averaged over the separation interval $0.04 h^{-1}\text{Mpc} \leq r_p < 10 h^{-1}\text{Mpc}$. In this case, the uncertainties determined using the method described in §3 apply to these averaged quantities: if γ and r_0 are thought to vary with separation, then their values at any particular separation are not

constrained by the error estimates for the separation-averaged values.

Figure 1 clearly demonstrates the correlation function depends strongly on SED class — early-type objects are more strongly clustered, and have a steeper slope, than late-type objects. Therefore, at least one of these samples must be a strongly biased tracer of the mass distribution. We parameterize the relative bias between the the early- and late-type samples according to the ratio of their correlation function amplitudes:

$$b_E/b_L = \sqrt{(r_0^\gamma)_E / (r_0^\gamma)_L}, \quad (7)$$

where the subscripts E and L denote quantities for the early- and late-type samples, respectively. The ratio of the early-type correlation function amplitude to that for the late-type objects is 2.9 ± 0.5 ; the relative bias is therefore $b_E/b_L = 1.7 \pm 0.2$. Note that, since the early- and late-type correlation functions have different slopes, the relative bias between the two samples is a power-law function of separation; the quantity b_E/b_L , as defined above, measures the amplitude of this function.

In Figure 2, we show how the amplitudes of the correlation functions for the early- and late-type samples depend on the SED number, s_{cut} , of the cutoff between the early- and late-type SED classes. We plot the quantity $r_0^{\gamma/1.73}$ vs. s_{cut} , where $r_0^{\gamma/1.73}$ is the correlation length scaled to $\gamma = 1.73$, the value for the full sample from Table 1. The scaled correlation length $r_0^{\gamma/1.73}$ is a measure of the amplitude of the correlation function, and allows us to compare the correlation lengths of different samples, independently of the slopes. The uncertainties in $r_0^{\gamma/1.73}$ are computed in the same manner as those in r_0 .

As expected, $r_0^{\gamma/1.73}$ for both samples decreases with s_{cut} , as objects are moved from the late-type sample to the early-type sample. This effect, however, is small compared to the difference between the clustering amplitudes of the two samples. Moreover, the relative bias changes by $\lesssim 10\%$ as s_{cut} is varied, and does not depend on s_{cut} in any systematic way. Our results are therefore not sensitive to the choice of cutoff SED number, and we adopt $s_{\text{cut}} = 0.5$ for the remainder of this paper.

4.2. Redshift Dependence

We next investigate how the correlation function for each SED class evolves with redshift. We divide each of the SED samples from §4.1 into SED-redshift subsamples, using the subsample parameters listed in Table 2. The redshift bins for each SED sample are chosen so that each bin contains approximately the same number of objects. This binning makes optimal use of the data; different redshift bins are considered in §4.3.

In Figure 3, we plot the projected correlation function $w_p(r_p)$ for each of the SED-redshift subsamples defined in Table 2; Figure 4 summarizes the dependence of $r_0^{\gamma/1.73}$ on median redshift. The excess correlation of the early-type objects relative to the late-type objects is present at all redshifts. Both the early- and late-type objects have a clustering amplitude which *increases* with

redshift. This is somewhat surprising, since a scenario in which the correlation function evolves due to gravitational instability would predict that the correlation function should increase, not decrease, with cosmic time. It therefore seems likely that the apparent evolution is actually evolution in the bias of our SED-redshift subsamples relative to the matter distribution, rather than an actual decay in the clustering of matter. The cause of this evolution in bias is discussed in §5.

In contrast to the strong evolution of the early- and late-type samples, the full sample undergoes little apparent evolution, consistent with earlier results (Small et al. 1999; Carlberg et al. 2000b; Hogg et al. 2000). However, as can be seen in Table 2, the ratio of the number of early-type objects to the number of late-type objects in our sample varies considerably with redshift; as similar variation is also present if the ratio is computed by weighing each object by the inverse of its selection function. The correlation function for data of all SED types will therefore exhibit apparent evolution, arising from the variation in the composition of the sample with redshift, in addition to any true evolution in clustering. For our selection criteria, the combined sample is composed of approximately equal numbers of early- and late-type objects at low redshifts, while at higher redshifts it is dominated by late-type galaxies. One would therefore expect that the correlation amplitude for the combined sample would approximate the average of the amplitudes for the early- and late-type samples at low redshifts, but more closely match the late-type amplitude at higher redshifts, as is observed.

To quantify the apparent evolution of the correlation function, we begin with the standard model

$$\xi_p(r; z) = \xi_p(r; 0)(1 + z)^{-(3+\epsilon)}, \quad (8)$$

(Groth & Peebles 1977), where $\xi_p(r; z)$ is the correlation function at physical, as opposed to comoving, separation r , and redshift z . In this model, $\epsilon = 0$ corresponds to clustering fixed in physical coordinates, and $\epsilon = \gamma - 3$ corresponds to a constant comoving correlation function. We employ equations (2) and (8) to obtain a model for the evolution of $r_0^{\gamma/1.73}$, the comoving correlation length scaled to our fiducial slope, $\gamma = 1.73$:

$$r_0^{\gamma/1.73}(z) = r_0^{\gamma/1.73}(0.3) \frac{(1+z)^{(\gamma(z)-3-\epsilon)/1.73}}{1.3^{(1.73-3-\epsilon)/1.73}}, \quad (9)$$

where the quantity $r_0^{\gamma/1.73}(0.3)$ is the correlation length at $z = 0.3$ scaled to $\gamma = 1.73$. We use $z = 0.3$, rather than $z = 0$, as our fiducial redshift, since $r_0^{\gamma/1.73}(0)$ is poorly constrained by our data.

Equation (8) is a purely empirical model, and is not necessarily expected to be valid at all redshifts. In particular, this model predicts a monotonic evolution of r_0 with redshift, at odds with both N -body simulation and observational results (Connolly, Szalay, & Brunner 1998; Baugh et al. 1999; Kauffmann et al. 1999). Thus, while the model does adequately describe our data, its predictions for r_0 at redshifts outside our observed range are to be treated with suspicion. Nonetheless, equation (8), applied to a limited range of redshifts, is a potentially useful model, due to the physical significance of the parameter ϵ .

We fit equation (9) to the SED-redshift subsample data, taking z to be the median redshift of the subsample. The results are given in Table 3; error contours for the fits are shown in Figure 5. Both the early- and late-type data are best modeled by a correlation amplitude which increases rapidly with redshift. The late-type data exclude a constant clustering strength ($\epsilon = \gamma - 3 = -1.27$) with 4σ confidence. The apparent evolution in the early-type sample is less rapid, but still only marginally consistent with $\epsilon = -1.27$. The correlation amplitude for the full sample, on the other hand, undergoes little apparent evolution, but is also consistent with $\epsilon = 0$, or no evolution in physical coordinates.

Our interpretation of these results is based on the estimated uncertainties in $r_0^{\gamma/1.73}$ and ϵ in Figure 5, which in turn depend on the estimated uncertainties in w_p from Table 2. The reliability of equation (4), with only four independent patches, is therefore an issue. In particular, the small size of the error bar for the low-redshift points for the early- and late-type SED-redshift subsamples, relative to the higher-redshift uncertainties, is a cause for some concern: insofar as the SED-redshift subsamples are identical, one would expect that the uncertainties in $r_0^{\gamma/1.73}$ would be the same for each subsample. However, while the sizes of the subsamples are similar, the selection functions are not: the higher-redshift subsamples are more sparsely sampled than their lower-redshift counterparts, and therefore one would expect that they would have larger uncertainties. Furthermore, the uncertainty depends on the correlation function: strongly clustered data will in general have a larger absolute uncertainty in the correlation amplitude than will weakly clustered data.

We test how the small uncertainty in $r_0^{\gamma/1.73}$ at low redshift affects our determination of $r_0^{\gamma/1.73}(0.3)$ and ϵ by re-fitting equation (9) to the early- and late-type SED-redshift data, with the uncertainties replaced by average values. We compute the averaged uncertainties in two ways: first, as the root-mean-square of the uncertainties in $r_0^{\gamma/1.73}$ from Table 2, and second, from the root-mean-square of the fractional uncertainties in $r_0^{\gamma/1.73}$. In both cases, the best-fitting $r_0^{\gamma/1.73}$ and ϵ agree with the values in Table 3 to within a few percent, and the confidence regions are actually somewhat smaller than those in Figure 5. Our best uncertainty estimates in Table 2, therefore, give the most conservative uncertainty estimates for $r_0^{\gamma/1.73}$ and ϵ . We conclude that our interpretation of the results shown in Figure 5 is not unduly affected by any unreliability in our estimated uncertainties in w_p .

We next consider the apparent evolution of γ with redshift. In Figure 6, we plot γ vs. median redshift for each of the SED-redshift samples. We model the evolution using a simple linear model

$$\gamma(z) = \gamma(0.3) + \beta_z(z - 0.3) . \tag{10}$$

The results of fitting equation (10) to the data are given in Table 3, and shown in Figure 7. We cannot place strong constraints on the evolution of γ for either the early- or the late-type SED samples: data from both samples are consistent with constant γ , or with γ being either a strongly increasing or a decreasing function of redshift. The full sample, on the other hand, does exhibit a significant decrease in γ with redshift. As with the apparent redshift dependence of the correlation

amplitude, however, this may be due to the large difference between the slopes of the early- and late-type correlation functions, and the redshift-dependent composition of the combined sample, rather than true evolution of γ .

4.3. Missing Variance

By subdividing the sample into many subsamples, we run the risk of underestimating the correlation function, due to the small volumes and numbers of objects being considered (Hamilton 1993). We test the significance of this in several ways. First, in Table 2, we compare r_0 for each SED-redshift subsample to the median, $r_{0\text{ med}}$, of the 4 correlation lengths determined from each patch individually, each scaled to the value of γ for that subsample. While $r_{0\text{ med}}$ is typically somewhat smaller than r_0 , in most cases this difference is not significant at the 1σ level. If the SED-redshift subsamples were small enough to be significantly affected by missing variance, one would expect the individual patches to be affected even more, and therefore have a significantly lower $r_{0\text{ med}}$.

Second, we consider SED-redshift subsamples constructed using larger redshift bins. Figure 8 shows $r_0^{\gamma/1.73}$ vs. redshift for the early- and late-type SED classes, both using the redshift bins in Table 2, and using overlapping bins obtained by combining data from adjacent bins. If the SED-redshift subsamples were significantly affected by missing variance, one would expect the estimated correlation amplitude for the larger bins to be greater than those for the two smaller bins. Again, no significant difference in clustering amplitude is found: the value of $r_0^{\gamma/1.73}$ for each overlapping bin is consistent with the average of the values for the two bins it comprises.

Finally, we note that if cosmic variance in the correlation function is significant for our subsamples, the fact that we use different redshift bins for the three SED samples could affect our results, since the SED-redshift subsamples sample different structures. To test the significance of this effect, we compute $r_0^{\gamma/1.73}$ for the early- and late-type samples with the same redshift bins as used for the combined sample. The results, plotted in Figure 9, are consistent with those obtained using the preferred equal-number bins. Since the clustering amplitude is not significantly affected by changing the subsample sizes, or by sampling different structures, we conclude that missing variance is not a serious problem in our sample.

4.4. Luminosity Dependence

To determine the luminosity dependence of the correlation function, we consider objects in the redshift range $0.12 \leq z < 0.40$; the SED subsamples are volume-limited for $M_R^0 < -19.25$ over this redshift range. We split these samples into M_R^0 bins, again chosen so that each SED- M_R^0 subsample has approximately the same number of objects. The sample parameters are given in Table 4.

Figure 10 shows $w_p(r_p)$ for each of the SED- M_R^0 subsamples; the dependence of $r_0^{\gamma/1.73}$ on median M_R^0 is shown in Figure 11. We model $r_0^{\gamma/1.73}(M_R^0)$ as a power-law:

$$r_0^{\gamma/1.73}(M_R^0) = r_0^{\gamma/1.73}(-20) \exp(-\kappa(M_R^0 + 20)/1.73) . \quad (11)$$

In this model, $r_0^{\gamma/1.73}(-20)$ is the correlation length at $M_R^0 = -20$, for $\gamma = 1.73$. The parameter κ describes the fractional variation in the correlation function amplitude with magnitude: $\kappa = -d \log \xi / dM_R^0$. The results of fitting this model to the data, taking M_R^0 to be the median magnitude of the subsample, are listed in Table 5; error contours for these fits are shown in Figure 12.

We find that the clustering amplitudes of the combined sample and of the early-type sample are weakly increasing functions of luminosity: $\kappa = 0.31 \pm 0.11$ and 0.35 ± 0.17 , respectively. The data from the late-type sample, on the other hand, are best modeled by an amplitude which is essentially independent of luminosity ($\kappa = -0.02 \pm 0.16$), although we cannot rule out a weak dependence on M_R^0 . As with the redshift dependence of the correlation function, the apparent luminosity dependence for the combined sample may be interpreted as being a manifestation of the color dependence, due to the varying SED composition of the sample with luminosity.

Finally, we consider variation of γ with M_R^0 . Figures 13 and 14 show γ vs. median M_R^0 for the SED- M_R^0 subsamples. As for the redshift dependence of γ , we use a linear model for the dependence on M_R^0 :

$$\gamma(M_R^0) = \gamma(-20) + \beta_M(M_R^0 + 20) . \quad (12)$$

The fit parameters $\gamma(-20)$ and β_M are listed in Table 5. As with the correlation amplitude, γ for the early-type and combined samples increases with luminosity at a moderate rate, while γ for the late-type sample is poorly constrained, but best modeled as being independent of luminosity. We note that, for the early-type and combined samples, γ is approximately independent of M_R^0 , except for the brightest subsamples, which have much larger values of γ than the fainter subsamples. Our simple model (12) may therefore not be entirely appropriate.

5. Discussion

5.1. Color Dependence

The strong dependence of clustering on SED indicates that galaxies are biased tracers of the mass distribution at $z \sim 0.4$, as is seen locally. Results from the Stromlo-APM Redshift Survey (Loveday et al. 1995), the Optical Redshift Survey (Hermit et al. 1996), the Las Campanas Redshift Survey (LCRS; Lin et al. 1996) and the Southern Sky Redshift Survey (SSRS2; Willmer et al. 1998) all indicate that, at $z \sim 0$, early-type objects are more strongly clustered, and have a steeper correlation function, than late-type galaxies. Quantitative comparisons between our results and those from these other surveys are difficult, due to differing selection criteria, and differing methods of quantifying the clustering. Nonetheless, local estimates of the relative biasing b_E/b_L range from 1.2 for the SSRS2, to 2.3 for the Stromlo-APM survey, similar to our value of 1.7 ± 0.2 .

A similar relative biasing has also been observed at higher redshifts. In the Canada-France Redshift Survey (CFRS), Le Fèvre et al. (1996) find $r_0 = 2.1 \pm 0.2 h^{-1} \text{Mpc}$ (measured in physical coordinates) for galaxies redder than the CWW Sbc SED, and $r_0 = 1.45 \pm 0.25 h^{-1} \text{Mpc}$ for blue objects over the redshift range $0.2 \leq z \leq 0.5$, where both fits were performed with γ fixed to 1.64. These correlation lengths are considerably smaller than those found for our data, possibly due to the small volumes and numbers of objects in the CFRS survey. The relative biasing of the two CFRS samples, however, is consistent with our result. Le Fèvre et al. find that the relative bias between their red and blue samples is considerably smaller for $0.5 \leq z \leq 0.8$ than it is for $0.2 \leq z \leq 0.5$. As is clear from Figure 4, we detect no trend towards lower relative biases at higher redshifts.

In the Norris survey, Small et al. (1999) find $r_0 = 4.46 \pm 0.19 h^{-1} \text{Mpc}$ and $\gamma = 1.84 \pm 0.07$ for weak [O II] emitters, and $r_0 = 3.80 \pm 0.40 h^{-1} \text{Mpc}$ and $\gamma = 1.85 \pm 0.18$ for strong [O II] sources, over the redshift range $0.2 \leq z \leq 0.5$, for a relative biasing of 1.2. The Norris survey strong-[O II] correlation amplitude is consistent with our late-type amplitude, but the weak-[O II] amplitude, and hence the relative biasing, is considerably smaller than our value for the early-type sample. Assessing the significance of this discrepancy is difficult, however, due to the different selection criteria.

5.2. Luminosity Dependence

Quantitative comparisons between surveys of the luminosity dependence of the correlation function are even more problematic than for the color dependence. In addition to different selection criteria for the different surveys, different authors determine the luminosity dependence of the correlation function in different ways. In the ESO Slice Project (ESP; Guzzo et al. 2000) and in the SSRS2, the luminosity dependence of the correlation function is determined from a series of concentric volume-limited samples of different sizes. Results from both surveys indicate a strong luminosity dependence of the correlation function amplitude: $\Delta \log \xi / \Delta M \sim -0.7$ for the ESP, and $\Delta \log \xi / \Delta M \sim -1$ for the SSRS2, although there is considerable variation with limiting magnitude for the latter survey. These measurements are not directly comparable to our κ , since $\Delta \log \xi / \Delta M$ expresses the fractional variation of the correlation function with the magnitude limit of the sample. One expects κ , determined from independent absolute magnitude bins, to be larger than $\Delta \log \xi / \Delta M$ computed from overlapping samples, and therefore the ESP and SSRS2 results indicate a luminosity dependence for the correlation amplitude which is much stronger than we observe here.

Strong luminosity dependence is also seen in the LCRS and in the Norris Survey. In these surveys, the luminosity dependence is determined by comparing the clustering amplitude of objects brighter than some cutoff magnitude to that for fainter objects. In the LCRS, galaxies brighter than $M_\star - 1$ are found to be $\sim 50\%$ more strongly clustered than fainter objects. For Norris Survey, the ratio of clustering amplitudes of objects brighter than M_\star to that for fainter objects is ~ 1.8 .

To compare these results to those from our survey, we average the clustering amplitudes of our two brightest bins, and those from the two faintest bins. The resulting cutoff magnitude, $M_R^0 = -20.10$, is close to M_* for both early- and late-type galaxies. We find that the bright galaxies are $\sim 35\%$ more strongly clustered than fainter objects, a smaller difference than seen in the LCRS and Norris surveys, but inconsistent with these results only at the 1σ level.

The methodology for determining the luminosity dependence of the correlation amplitude for the Stromlo-APM Survey most closely matches our own, as do the results. Using independent, volume-limited samples, selected jointly in absolute magnitude and morphology, with $M_B < -17$, Loveday et al. (1995) find $\Delta \log \xi / \Delta M \sim -0.25$ for early-type objects, and $\Delta \log \xi / \Delta M \sim -0.15$ for late type objects. These values are reduced to ~ -0.10 for both morphological types, if the sample is restricted to objects brighter than $M_B = -19.5$. These measurements are in good agreement with our results, $d \log \xi / dM = -0.35 \pm 0.17$ and 0.02 ± 0.16 for objects with early- and late-type SEDs, respectively.

5.3. Redshift Dependence

The unphysical evolution of the correlation function observed for the early- and late-type SED samples is almost certainly caused by evolution of the galaxies themselves, rather than true decay in clustering. However, while galaxy evolution is found to cause the galaxy correlation function to increase with redshift in semi-analytic models (Baugh et al. 1999; Kauffmann et al. 1999) this effect is generally limited to high redshifts. For $z < 0.5$, in their Λ CDM model (Figure 7), Kauffmann et al. find that the correlation function of galaxies with high star formation rates decreases rapidly with redshift, inconsistent with the evolution seen in our late-type SED sample. The correlation function of the Kauffmann et al. early-type morphology sample, on the other hand, slowly increases with redshift at low redshifts. While this behavior is qualitatively similar to that of our early-type SED sample, the evolution in the Kauffmann et al. early-type morphology sample is considerably less rapid than that in our sample. As a result, the correlation amplitude of early-type galaxies predicted by the model is $\sim 50\%$ greater at $z = 0.2$ than is observed here. Of course, one would not necessarily expect the evolution of clustering in SED-selected samples to match precisely that seen in samples selected by star formation rate or by morphology. The fact that the clustering in our SED-selected samples continues to decay at low redshifts would therefore seem to indicate that the physical nature of the galaxies in our samples is still evolving at $z \sim 0.2$.

One form of galaxy evolution which can produce a correlation amplitude which decreases with cosmic time is galaxy merging. However, the merger rate varies approximately as $(1+z)^{-\epsilon}$, and so would need to be much greater than is observed (Carlberg et al. 2000a; Patton et al. in preparation) in order to explain our results. Another, more likely, explanation is color evolution.

As discussed in §2.1, the use of non-evolving template SEDs for galaxy classification can result in some higher-redshift galaxies being systematically misclassified as later types, so that

our selection criteria do not select a set of objects whose properties are independent of redshift. Assuming our SED classifications correspond roughly to morphological types at $z = 0$, the early-type SED sample will comprise all E/S0 objects at low redshifts, but at higher redshifts, only those ellipticals which do not undergo significant color evolution. The late-type SED sample, on the other hand, will contain objects of later morphological types at all redshifts, but the high-redshift late-type subsamples will also include those E/S0 objects which do undergo significant color evolution.

A simple evolution scenario, in which the average color evolution experienced by a galaxy depends only on that galaxy’s unevolved SED, or its morphological type, probably cannot explain the apparent evolution of the correlation function, however. Misclassifying some high-redshift elliptical galaxies as having later-type SEDs would cause an apparent increase with redshift in the correlation amplitude for our late-type SED sample, but would not affect the observed evolution of the early-type clustering. Although it is unlikely, since the CWW template SEDs are compiled from the spectra of local galaxies, the template SEDs could also be too blue, in which case our low-redshift early-SED subsamples would contain some galaxies of later unevolved types. While this would explain the apparent decrease with cosmic time of the early-type correlation amplitude, it would also result in a relative bias between unevolved early- and late-type objects at low redshifts which is much greater than is observed.

If color evolution is to explain the apparent clustering evolution, we require that the color evolution experienced by a galaxy be correlated with the galaxy correlation function. As an example, suppose that E/S0 objects which undergo sufficient color evolution to be classified as having late-type SEDs at $z \sim 0.5$ are for some reason less strongly clustered than those ellipticals with non-evolving colors (but still more strongly clustered than objects of later morphological types). Both the early- and late-type high-redshift SED subsamples will therefore contain objects which are more strongly clustered than those in their low-redshift counterparts, resulting in an apparent increase with redshift of the correlation function amplitude for both types.

One possibility is that E/S0 objects which undergo significant color evolution have smaller masses than those whose SEDs do not evolve. Since low-mass objects are expected to cluster less strongly than high mass objects, E/S0 galaxies with non-evolving SEDs would be more strongly clustered than those with evolving SEDs, resulting in the observed evolution of r_0^γ . Assuming that more massive E/S0 objects are also more luminous, this scenario is consistent with the apparent luminosity dependence of the correlation function, and could also explain the evolution of the luminosity function, as reported in Lin et al. (1999), where the early-type SED sample undergoes strong luminosity evolution, while the late-type sample is subject to strong number evolution.

Another possible connection between color evolution and clustering is galaxy age. Elliptical galaxies which formed sufficiently early in the history of the universe have presumably stopped evolving by $z \sim 0.5$. E/S0 objects formed at later epochs, on the other hand, might still have significantly bluer SEDs at $z \sim 0.5$ than those at $z = 0$. However, galaxies which form at early

epochs are expected to be more strongly clustered than those formed at later epochs, since the peaks in the matter distribution are rarer at higher redshifts than at lower redshifts, and therefore more strongly biased (Kaiser 1984). Older ellipticals experiencing less color evolution than young ones could therefore also explain the observed evolution of r_0^γ .

Of course, other mechanisms may be responsible for the relationship between the correlation function and the color evolution rate, and the relationship may not be that described in the example above. We stress, however, that regardless of the details, if color evolution is the cause of the apparent evolution of the correlation function, then the color evolution rate must be in some way correlated with the galaxy correlation function. This argument may be inverted: if the apparent evolution of clustering of a sample of galaxies is to be assigned a clear physical interpretation, then the selection criteria of that sample must be based on galaxy properties which are either independent of redshift, or depend on redshift in a manner which is unrelated to the correlation function. The foregoing considerations make clear that defining such a sample is likely to be difficult, since the galaxy properties used to define the sample (such as luminosity and SED) are quite likely to evolve, and it is plausible that the evolution of these properties does depend on the correlation function.

6. Summary

We have investigated how the correlation function depends on galaxy color, redshift and luminosity, using volume-limited, evolution-compensated samples from the CNOC2 redshift survey. Galaxies are classified according to their spectral energy distributions, using non-evolving template SEDs. The samples considered appear to be large enough to avoid being significantly affected by missing variance.

The correlation function depends strongly on SED: early-type objects are more strongly clustered, and have a steeper correlation function slope, than late-type objects. We find $r_0 = 5.45 \pm 0.28 h^{-1} \text{Mpc}$, $\gamma = 1.91 \pm 0.06$ for early-type objects, and $r_0 = 3.95 \pm 0.12 h^{-1} \text{Mpc}$, $\gamma = 1.59 \pm 0.08$ for late-type galaxies, over the redshift range $0.12 \leq z < 0.51$. The combined sample (both early- and late-type objects) has $r_0 = 4.54 \pm 0.22 h^{-1} \text{Mpc}$ and $\gamma = 1.73 \pm 0.02$. The relative bias of the early- and late-type samples is $b_E/b_L = 1.7 \pm 0.2$; a large relative bias exists at all redshifts in the sample.

The correlation amplitude for early-type objects increases at a moderate rate with luminosity, $d \log \xi / dM_R^0 = -0.35 \pm 0.17$, while that for late-type galaxies has no significant luminosity dependence: $d \log \xi / dM_R^0 = 0.02 \pm 0.16$. The slope of the early-type correlation function also depends on luminosity, with γ being largest for the brightest subsample; γ for the late-type sample is best modeled as being independent of luminosity, although this result is poorly constrained. The luminosity dependence of the correlation function for the combined sample is similar to that for the early-type sample. However, the SED composition of the combined sample varies with luminosity, and so the apparent luminosity dependence of this sample is at least in part caused by the strong

color dependence.

Both early- and late-type objects have clustering amplitudes which appear to increase rapidly with redshift: $\epsilon = -3.9 \pm 1.0$ for early-type objects, $\epsilon = -7.7 \pm 1.3$ for late types. While the dependence of γ on z for both these samples is consistent with no evolution, we cannot place strong constraints on its behavior. The combined sample, on the other hand, shows little evolution in amplitude, with $\epsilon = -2.1 \pm 1.3$, but a significant decrease in γ with redshift. This apparent discrepancy may be explained by the varying SED composition of the full sample with redshift.

If our SED-redshift subsamples represent populations of objects with physical properties which are independent of redshift, the observed evolution of the amplitude of the correlation function is inconsistent with a scenario in which gravitational instability drives the formation and evolution of structure. However, if galaxy colors have undergone significant evolution since $z \sim 0.5$, then our use of non-evolving template SEDs may mean that our selection criteria are not in fact independent of redshift. If the color evolution experienced by a galaxy is correlated with the galaxy correlation function, then color evolution could explain the apparent increase in clustering amplitude with redshift.

Even if colour evolution is significant, our results on the joint SED-redshift dependence of the correlation function, as shown in Figure 4, still serve as a model-independent description of the apparent evolution of galaxy clustering as a function of galaxy SED. Two important conclusions may be drawn from these results, independent of any particular colour evolution model. Firstly, there is a large range of clustering bias over the entire redshift range $0.12 \leq z < 0.51$. Secondly, galaxy evolution makes a major contribution to the apparent evolution of galaxy clustering. It is therefore extremely difficult to construct a galaxy sample which traces the mass distribution in a way which is independent of redshift, as is necessary if physical conclusions about the evolution of the mass correlation function are to be obtained directly from galaxy survey data.

This project was supported by a collaborative program grant from NSERC, as well as individual operating grants from NSERC to RGC and HKCY. HL Acknowledges support provided by NASA through Hubble Fellowship grant #HF-01110.01-98A awarded by the Space Telescope Science Institute, which is operated by the Association of Universities for Research in Astronomy, Inc., for NASA under contract NAS 5-26555.

REFERENCES

- Baugh, C. M., Benson, A. J., Cole, S., Frenk, C. S., & Lacey, C. G. 1999, *MNRAS*, 305, L21
- Carlberg, R. G., Yee, H. K. C., Morris, S. L., Lin, H., Sawicki, M., Wirth, G., Patton, D., Shepherd, C. W., Ellingson, E., Schade, D., Pritchet, C. J., & Hartwick, F. D. A. 1998, *Phil. Trans. Roy. Soc. Lond. A.*, 357, 167

- Carlberg, R. G., Cohen, J. G., Patton, D. R., Blandford, R., Hogg, D. W., Yee, H. K. C., Morris, S. L., Lin, H., Hall, P. B., Sawicki, M., Wirth, G. D., Cowie, L. L., Hu, E., & Songailia, A. 2000a, *ApJ*, 352, L1
- Carlberg, R. G., Yee, H. K. C., Morris, S. L., Lin, H., Hall, P., Patton, D., Sawicki, M., & Shepherd, C. W. 2000b, *ApJ*, 542, 57
- Cole, S., Ellis, R., Broadhurst, T., & Colless, M. 1994, *MNRAS*, 267, 541
- Coleman, G. D., Wu, C., & Weedman, D. W. 1980, *ApJS*, 43, 393
- Connolly, A. J., Szalay, A. S., & Brunner, R. J. 1998, *ApJ*, 499, L125
- Groth, E. J., & Peebles, P. J. E. 1977, *ApJ*, 217, 385
- Guzzo, L., Bartlett, J. G., Cappi, A., Maurogordato, S., Zucca, E., Zamorani, G., Balkowski, C., Blanchard, A., Cayatte, V., Chincarini, G., Collins, C. A., Maccangi, D., MacGillivray, H., Merighi, R., Mignoli, R., Proust, D., Ramella, M., Scaramella, R., Stirpe, G. M., & Vettolani, G. 2000, *A&A*, 355, 1
- Hamilton, A. J. S. 1993, *ApJ*, 417, 19
- Hermit, S., Santiago, B. X., Lahav, O., Strauss, M. A., Davis, M., Dressler, A., & Huchra, J. P. 1996, *MNRAS*, 283, 709
- Hogg, D. W., Cohen, J. G., & Blandford, R. 2000, *ApJ*, 545, 32
- Kaiser, N. 1984, *ApJ*, 284, L9
- Kauffmann, G., Colberg, J. M., Diaferio, A., & White, S. D. M. 1999, *MNRAS*, 307, 529
- Le Fèvre, O., Hudon, D., Lilly, S. J., Crampton, D., Hammer, F., & Tresse, L. 1996, *ApJ*, 461, 534
- Lin, H., Kirshner, R. P., Schectman, S. A., Landy, S. D., Oemler, A., Tucker, D. L., & Schecter, P. L. 1996, *ApJ*, 471, 617
- Lin, H., Yee, H. K. C., Carlberg, R. G., Morris, S. L., Sawicki, M., Patton, D. R., Wirth, G., & Shepherd, C. W. 1999, *ApJ*, 518, 533
- Loveday, J., Maddox, S. J., Efstathiou, G., & Peterson, B. A. 1995, *ApJ*, 442, 457
- Matarrese, S., Coles, P., Lucchin, F., & Moscardini, L. 1997, *MNRAS*, 286, 115
- Mo, H. J., & White, S. D. M. 1996, *MNRAS*, 282, 347
- Peebles, P. J. E. 1980, *The Large-Scale Structure of the Universe* (Princeton: Princeton Univ. Press)
- Small, T. A., Ma, C., Sargent, W. L. W., & Hamilton, D. 1999, *ApJ*, 524, 31

Willmer, C. N. A., Da Costa, L. N., & Pellegrini, P. S. 1998, *AJ*, 115, 869

Yee, H. K. C., Ellingson, E., & Carlberg, R. G. 1996, *ApJS*, 102, 269

Yee, H. K. C., Morris, S. L., Lin, H., Carlberg, R. G., Hall, P. B., Sawicki, M., Patton, D. R.,
Wirth, G. D., Ellingson, E., & Shepherd, C. W. 2000, *ApJS*, 129, 475

This preprint was prepared with the AAS L^AT_EX macros v5.0.

Table 1. SED Sample Correlation Function Parameters

SED ^a	z_{med}	N	r_0^{b}	γ^{b}
All	0.375	1993	4.54 ± 0.22	1.73 ± 0.02
Early	0.338	720	5.45 ± 0.28	1.91 ± 0.06
Late	0.392	1273	3.95 ± 0.12	1.59 ± 0.08

^aAll samples have $M_R^0 < -20$ and $0.12 \leq z < 0.51$.

^bOne-parameter 1σ confidence intervals.

Table 2. SED-Redshift Subsample Correlation Function Parameters

SED ^a	$z_{\text{min}}, z_{\text{max}}$	z_{med}	N^{b}	r_0^{c}	γ^{c}	$r_0^{\gamma/1.73\text{c}}$	$r_{0\text{med}}^{\text{d}}$
All	0.120, 0.292	0.228	499 (275+224)	3.75 ± 0.23	1.87 ± 0.15	4.17 ± 0.49	3.73
	0.292, 0.375	0.350	493 (189+304)	3.87 ± 0.64	1.82 ± 0.16	4.15 ± 0.47	3.28
	0.375, 0.438	0.398	502 (156+346)	4.26 ± 0.15	1.65 ± 0.07	3.98 ± 0.28	4.05
	0.438, 0.510	0.469	499 (100+399)	5.14 ± 0.56	1.53 ± 0.09	4.25 ± 0.29	4.96
Early	0.120, 0.270	0.221	248	4.12 ± 0.20	2.05 ± 0.08	5.35 ± 0.20	3.90
	0.270, 0.382	0.350	234	5.30 ± 1.04	1.95 ± 0.16	6.55 ± 1.16	4.28
	0.382, 0.510	0.426	238	4.96 ± 0.62	2.10 ± 0.11	6.99 ± 0.57	4.63
Late	0.120, 0.324	0.258	321	2.41 ± 0.24	1.68 ± 0.08	2.35 ± 0.23	2.61
	0.324, 0.392	0.366	314	3.24 ± 0.60	1.74 ± 0.30	3.26 ± 0.82	3.05
	0.392, 0.453	0.418	322	4.51 ± 0.70	1.60 ± 0.08	4.03 ± 0.71	3.82
	0.453, 0.510	0.473	316	4.65 ± 0.53	1.59 ± 0.12	4.11 ± 0.25	4.29

^aAll subsamples have $M_R^0 < -20$.

^bThe numbers in parentheses for the combined subsamples are the number of early-type and late-type galaxies comprised by the subsample.

^cOne-parameter 1σ confidence intervals.

^dThe median of the scaled correlation lengths from the individual patches. See §4.3 for details.

Table 3. Correlation Function Redshift Dependence

SED	$r_0^{\gamma/1.73}(z = 0.3)^a$	ϵ^a	$\gamma(z = 0.3)^a$	β_z^a
All	4.1 ± 0.3	-2.1 ± 1.3	1.8 ± 0.1	-1.5 ± 0.7
Early	5.7 ± 0.2	-3.9 ± 1.0	2.0 ± 0.1	0.1 ± 0.6
Late	2.7 ± 0.2	-7.7 ± 1.3	1.7 ± 0.1	-0.4 ± 0.6

^aThe tabulated uncertainties are the one-parameter 1σ confidence intervals. See Figures 5 and 7 for the joint two-parameter confidence regions.

Table 4. SED- M_R^0 Subsample Correlation Function Parameters

SED ^a	$M_{R\min}^0, M_{R\max}^0$ ^b	$M_{R\text{med}}^0$	N^c	r_0^d	γ^d	$r_0^{\gamma/1.73d}$
All	-22.52, -20.60	-20.99	576 (292+284)	3.68 ± 0.31	1.92 ± 0.06	4.25 ± 0.28
	-20.60, -20.10	-20.31	554 (215+339)	3.74 ± 0.25	1.68 ± 0.09	3.60 ± 0.23
	-20.10, -19.65	-19.88	557 (188+369)	3.25 ± 0.27	1.81 ± 0.13	3.43 ± 0.16
	-19.65, -19.25	-19.46	542 (113+429)	3.52 ± 0.51	1.65 ± 0.08	3.32 ± 0.44
Early	-22.52, -20.65	-21.11	278	4.66 ± 0.34	2.14 ± 0.02	6.71 ± 0.53
	-20.65, -20.00	-20.27	276	4.68 ± 0.08	1.89 ± 0.06	5.40 ± 0.19
	-20.00, -19.25	-19.68	254	5.19 ± 0.73	1.85 ± 0.08	5.82 ± 0.81
Late	-22.27, -20.45	-20.83	352	3.11 ± 0.36	1.58 ± 0.25	2.82 ± 0.27
	-20.45, -20.00	-20.21	359	2.86 ± 0.18	1.71 ± 0.16	2.83 ± 0.26
	-20.00, -19.60	-19.79	345	3.22 ± 0.55	1.67 ± 0.16	3.09 ± 0.54
	-19.60, -19.25	-19.42	365	2.95 ± 0.27	1.67 ± 0.15	2.84 ± 0.27

^aAll subsamples have $0.12 \leq z < 0.40$.

^b $M_{R\min}^0$ for the brightest bin for each SED class is taken to be the M_R^0 of the brightest object of that class.

^cThe numbers in parentheses for the combined subsamples are the number of early-type and late-type galaxies comprised by the subsample.

^dOne-parameter 1σ confidence intervals.

Table 5. Correlation Function Absolute Magnitude Dependence

SED	$r_0^{\gamma/1.73}(M_R^0 = -20)^a$	κ^a	$\gamma(M_R^0 = -20)^a$	β_M^a
All	3.50 ± 0.12	0.31 ± 0.11	1.73 ± 0.04	-0.17 ± 0.06
Early	5.19 ± 0.24	0.35 ± 0.17	1.87 ± 0.04	-0.24 ± 0.05
Late	2.85 ± 0.14	-0.02 ± 0.16	1.67 ± 0.08	0.03 ± 0.18

^aThe tabulated uncertainties are the one-parameter 1σ confidence intervals. See Figures 12 and 14 for the joint two-parameter confidence regions.

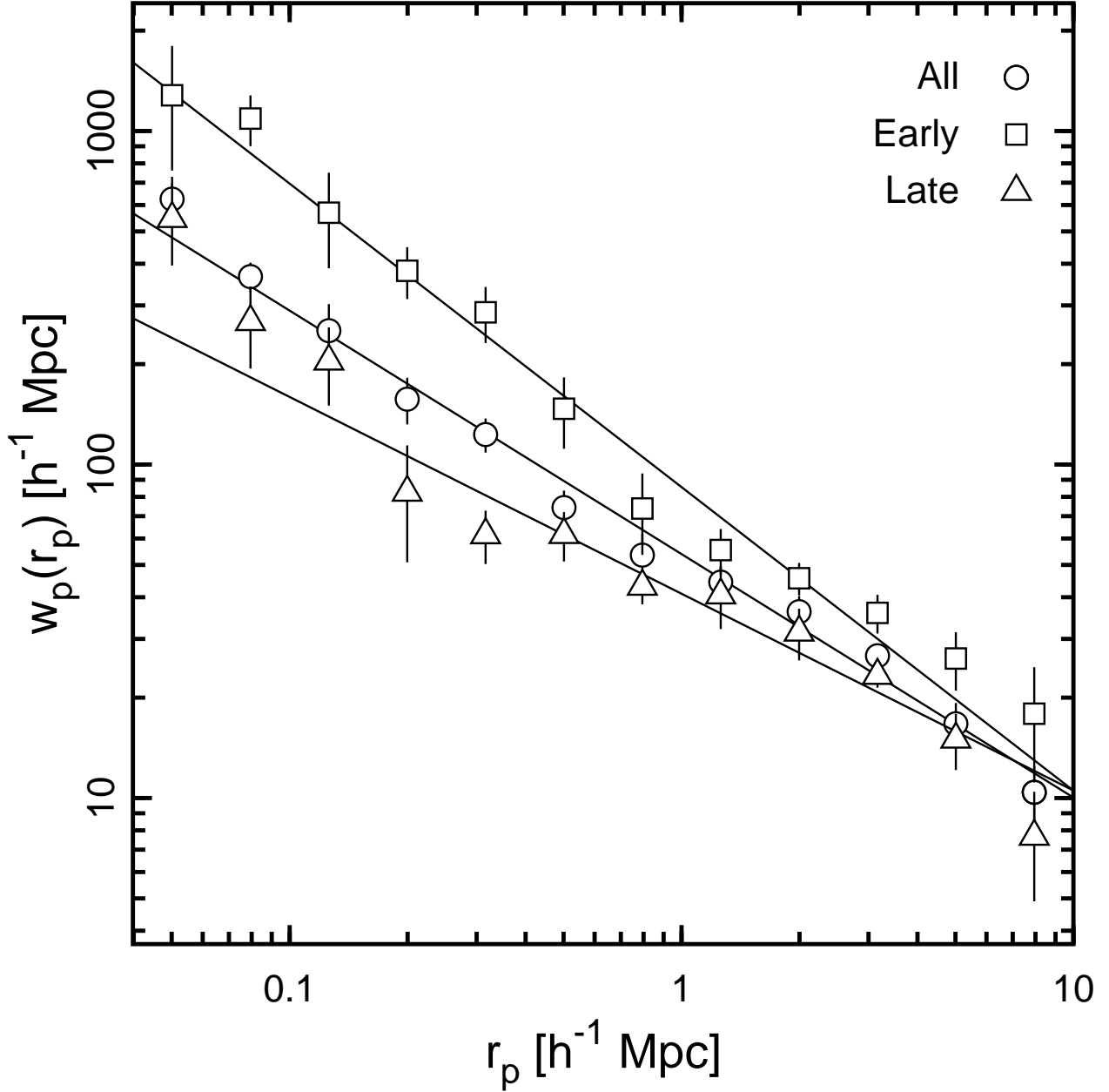


Fig. 1.— Projected comoving correlation function $w_p(r_p)$ for objects with $M_R^0 < -20$ and $0.12 \leq z < 0.51$, from all SED classes, and the early- and late-type SED classes individually. The lines show the model (equation 2), fit to the data for each sample. The fit parameters are given in Table 1.

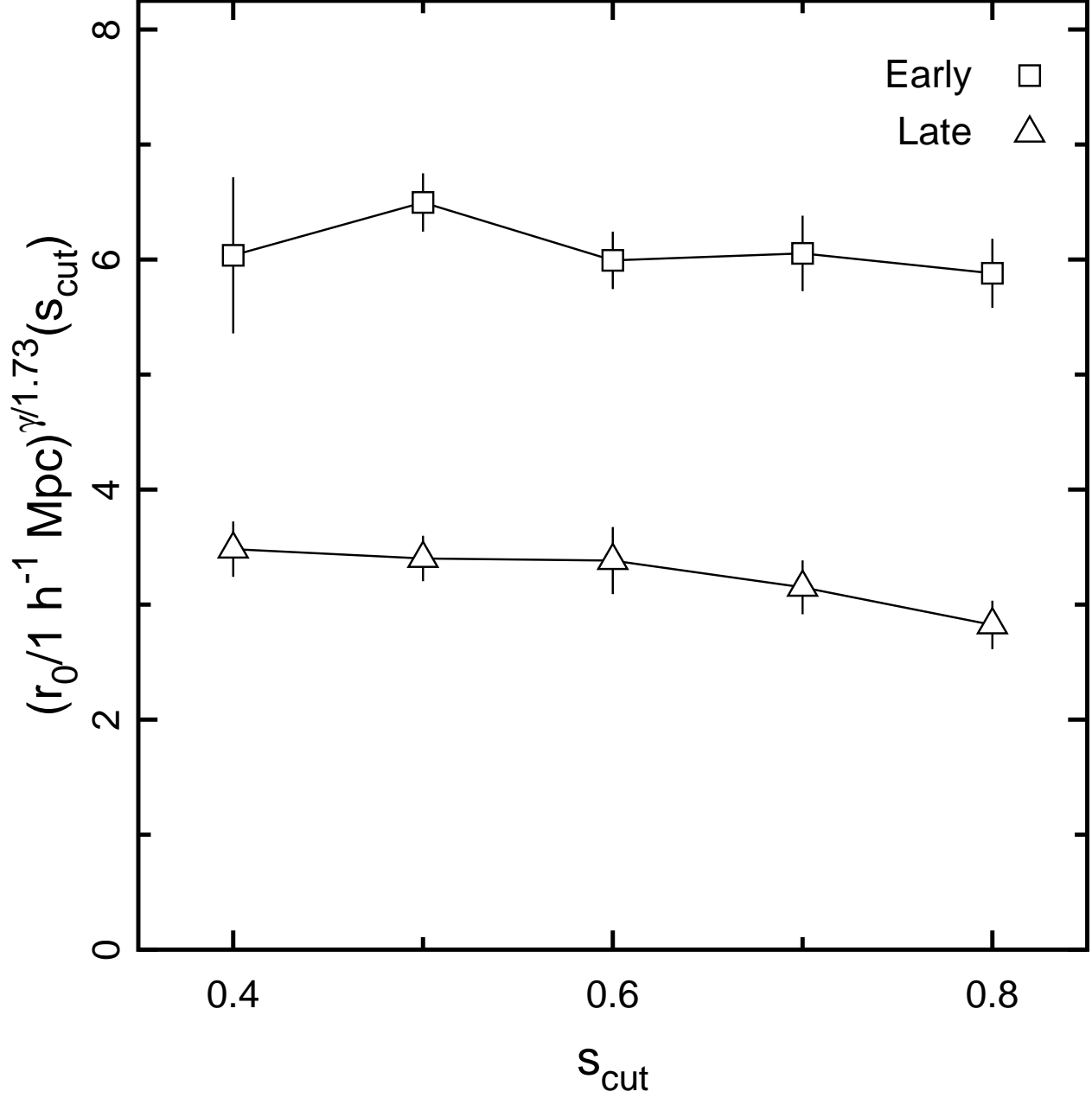


Fig. 2.— Scaled comoving correlation length $r_0^{\gamma/1.73}$ vs. cutoff SED number s_{cut} for the early- and late-type SED samples. For each cutoff s_{cut} , the early- and late-type SED samples consist of those objects with $-0.5 \leq s < s_{\text{cut}}$, and $s_{\text{cut}} \leq s < 3.5$, respectively.

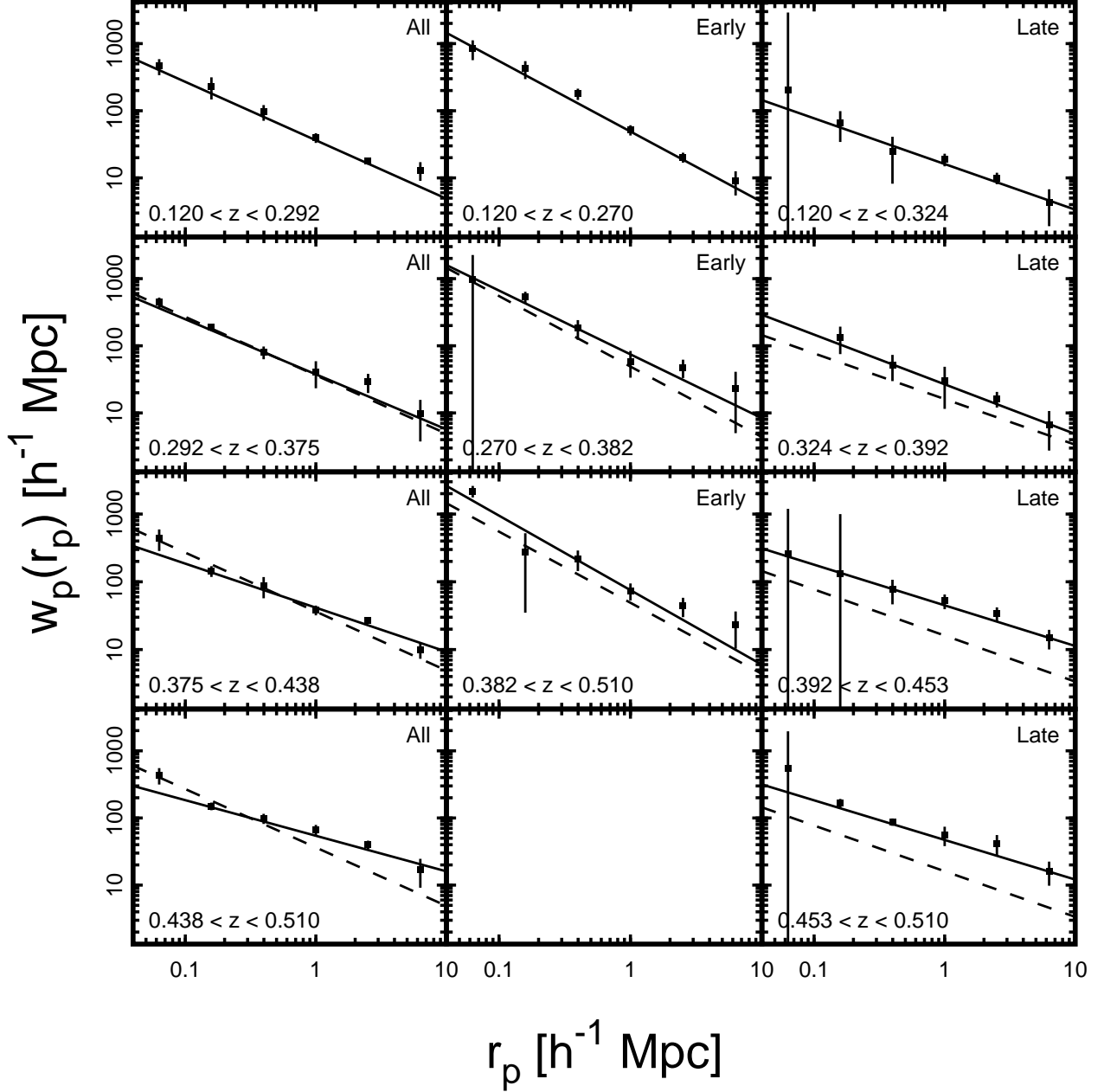


Fig. 3.— Projected comoving correlation function $w_p(r_p)$ for each of the SED-redshift subsamples. The solid line in each panel is the model (equation 2), fit to the data for that subsample; the fit parameters are given in Table 2. The dashed lines show the model from the lowest-redshift subsample for each SED class.

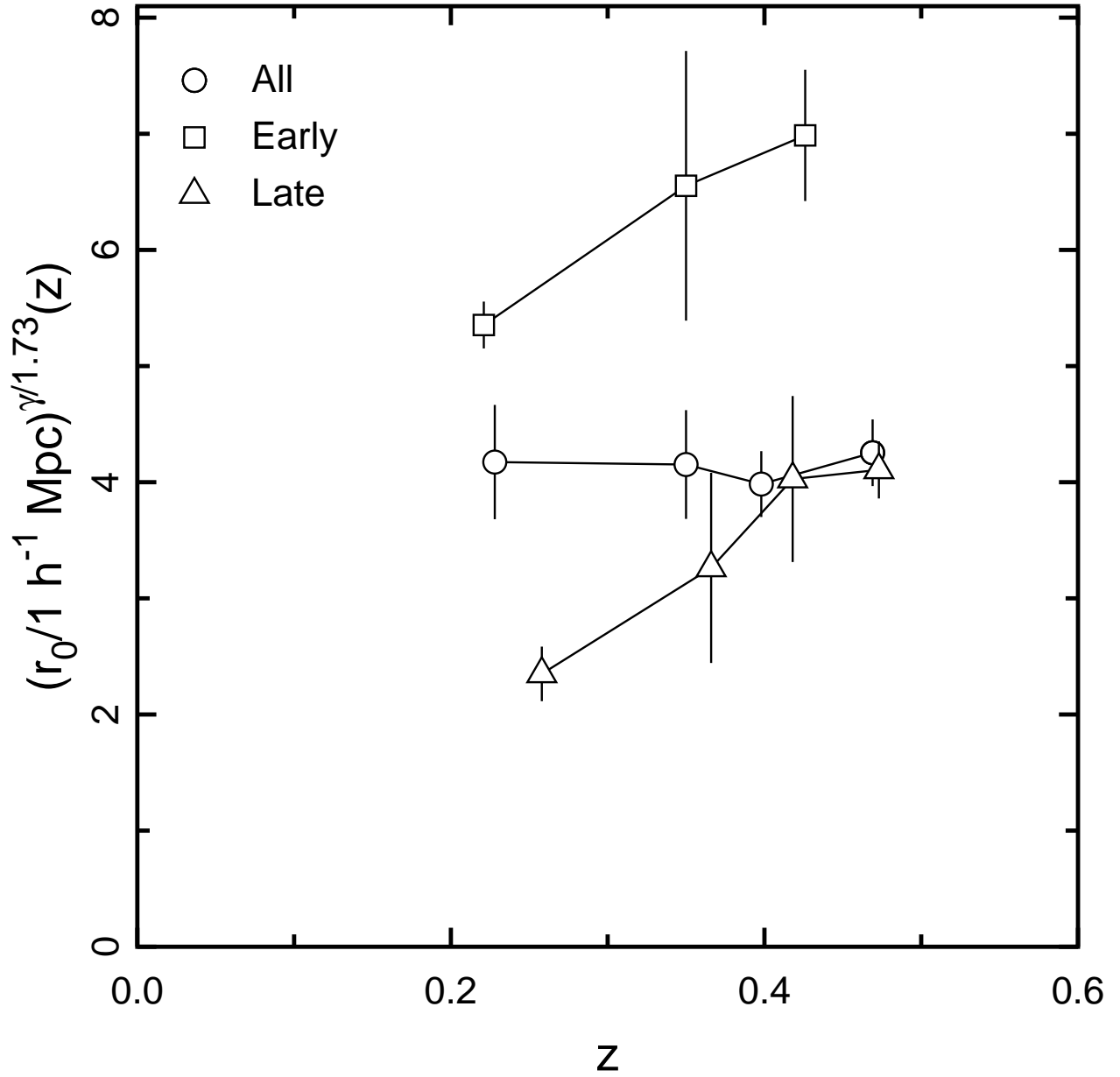


Fig. 4.— Scaled comoving correlation length $r_0^{\gamma/1.73}$ vs. median redshift for each SED-redshift subsample. Each subsample has $M_R^0 < -20$.

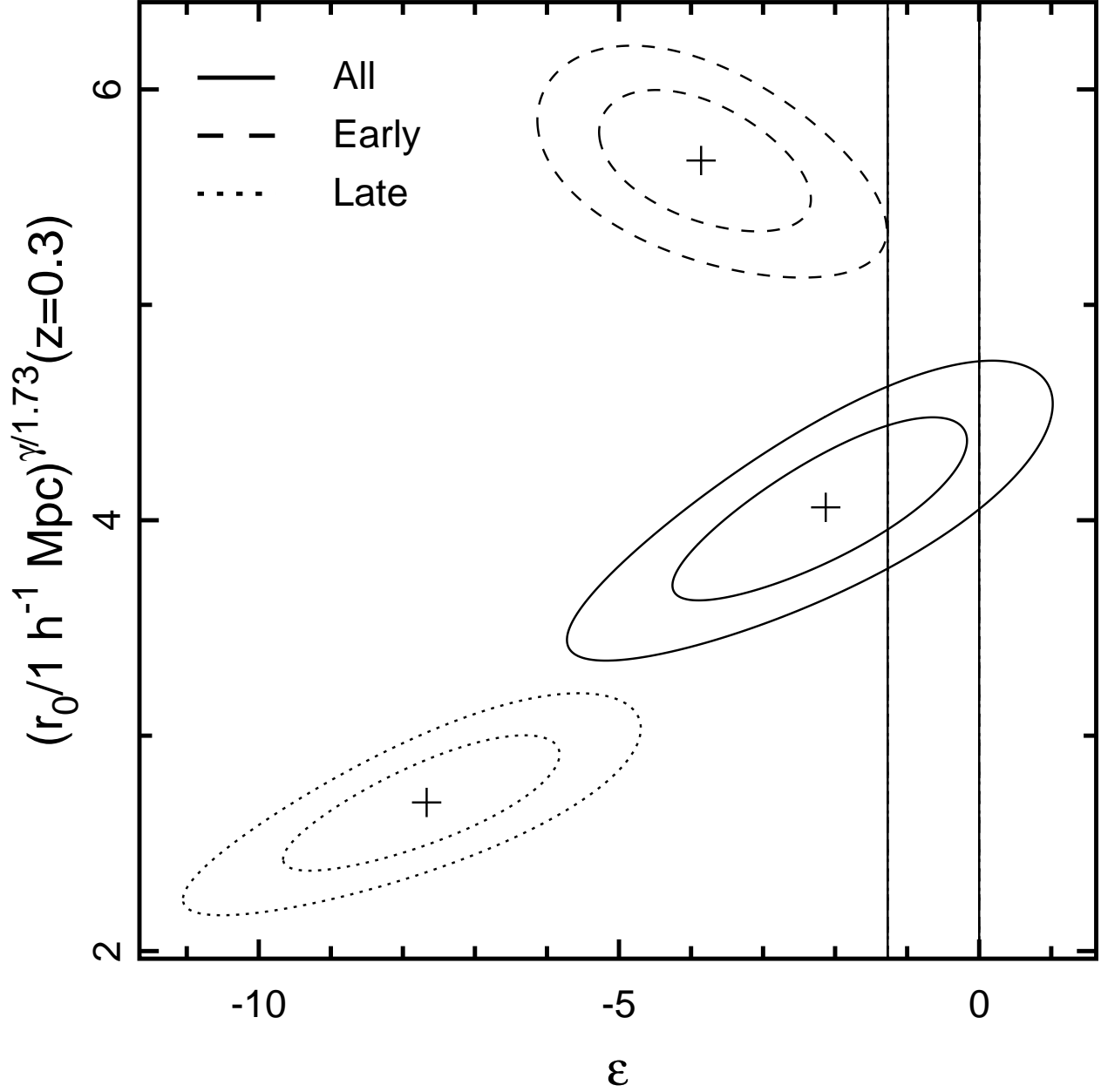


Fig. 5.— One- and 2σ ($\Delta\chi^2 = 2.30$ and 6.17) error contours for the fits of equation (9) for the SED-redshift subsamples. The leftmost vertical line corresponds to $\epsilon = 1.73 - 3 = -1.27$, or no evolution in comoving coordinates. The rightmost vertical line is $\epsilon = 0$, or no evolution in physical coordinates.

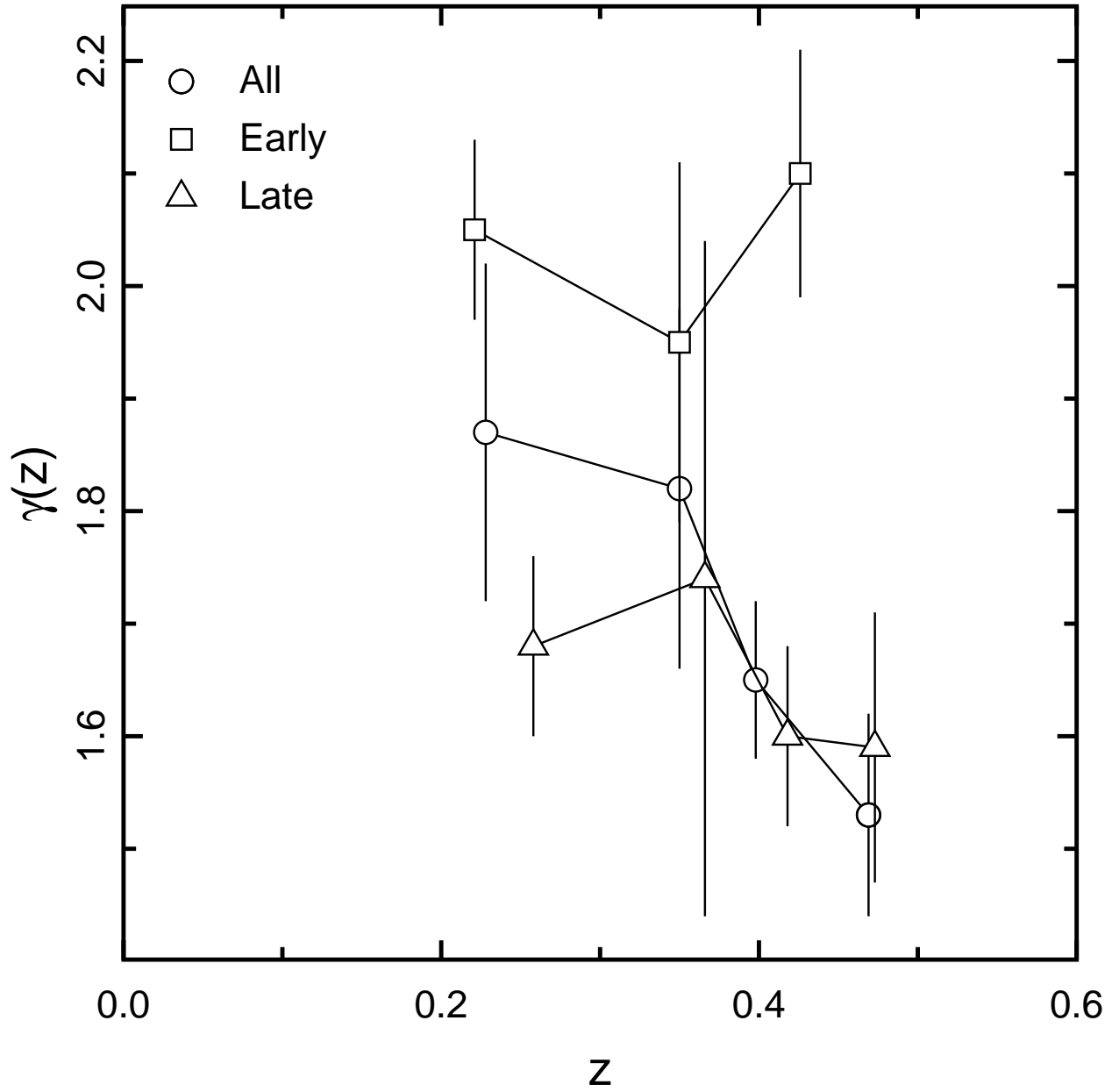


Fig. 6.— Correlation function slope γ vs. median redshift for the SED-redshift subsamples.

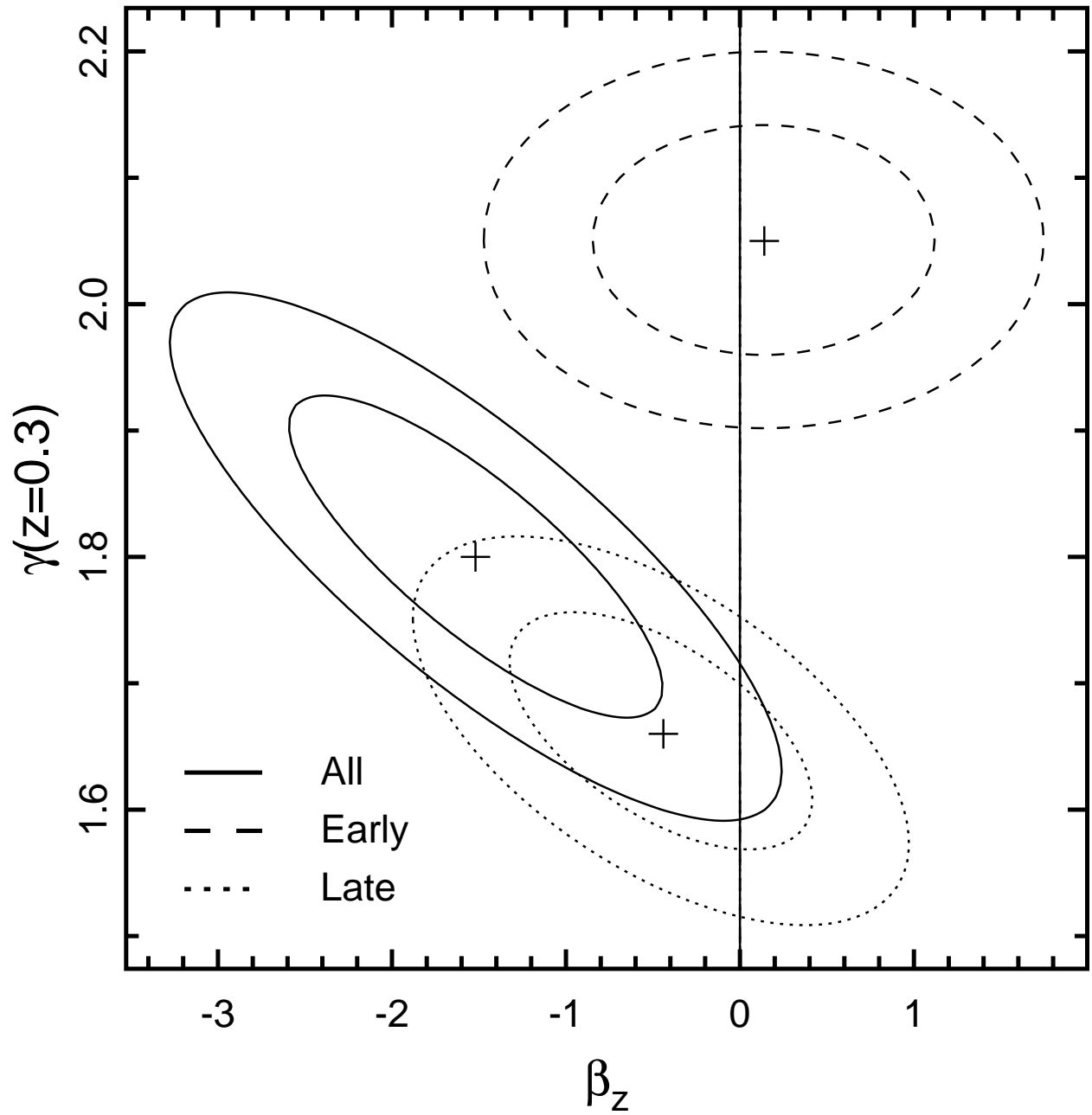


Fig. 7.— One- and 2σ ($\Delta\chi^2 = 2.30$ and 6.17) error contours for the fits of equation (10) for the SED-redshift subsamples.

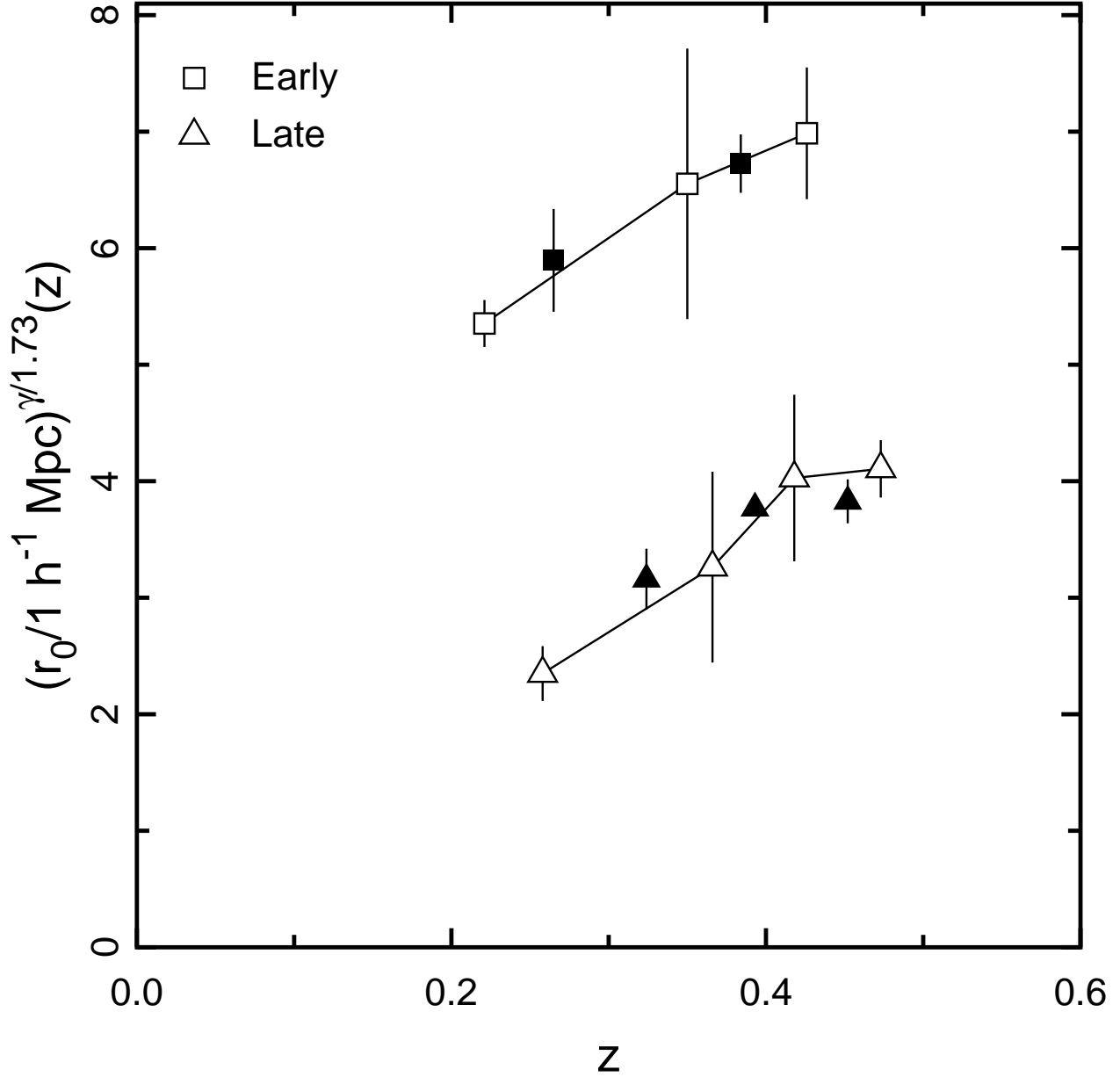


Fig. 8.— Scaled comoving correlation length $r_0^{\gamma/1.73}$ for the early- and late-type SED-redshift subsamples, for different choices of redshift bins. The open symbols are $r_0^{\gamma/1.73}$ computed using the redshift bins listed in Table 2; these are the same data as shown in Figure 4. The filled symbols are $r_0^{\gamma/1.73}$ computed for overlapping redshift bins constructed by combining data from adjacent bins — see §4.3 for details.

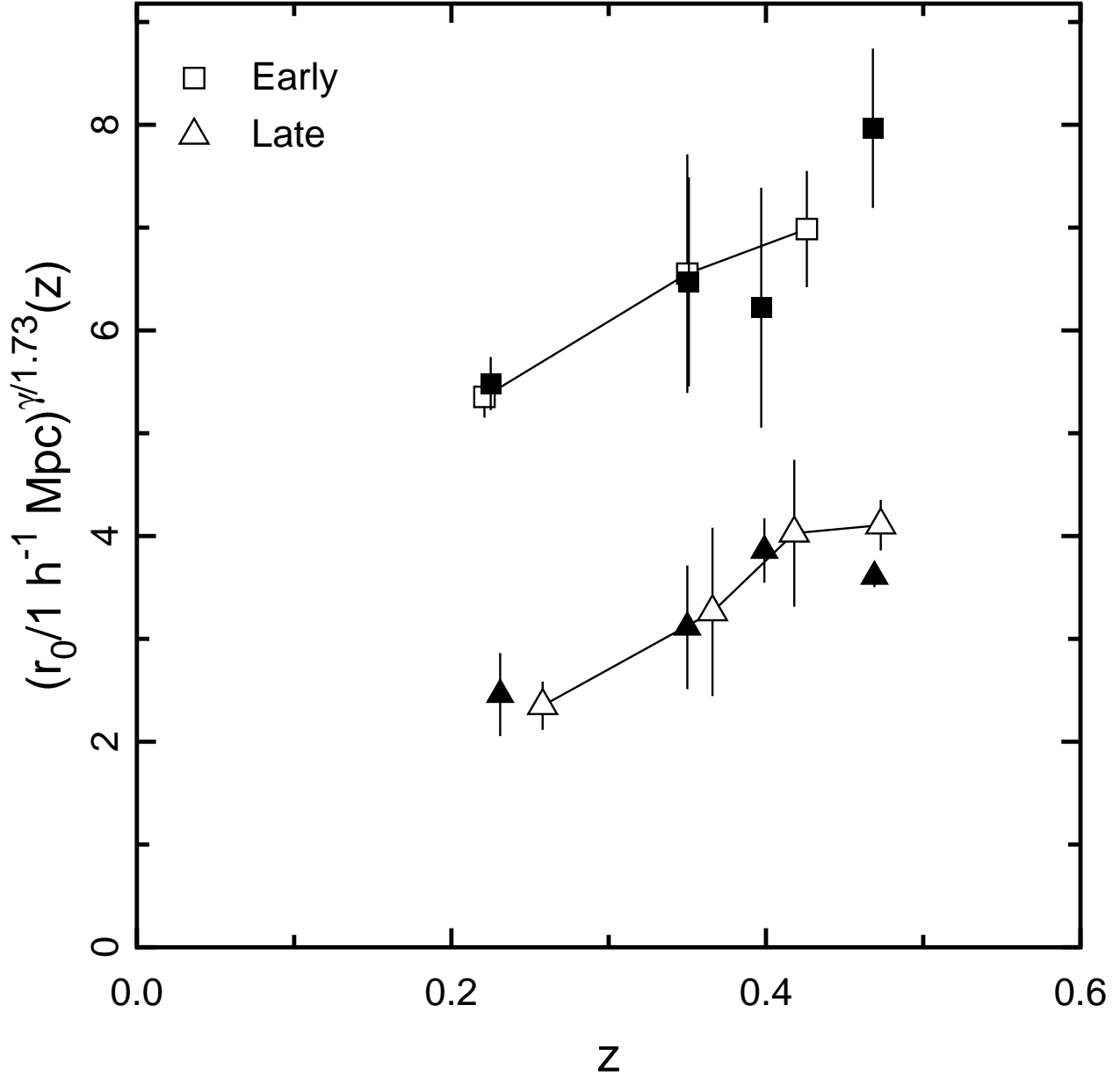


Fig. 9.— Scaled comoving correlation length $r_0^{\gamma/1.73}$ for the early- and late-type SED-redshift subsamples, for different choices of redshift bins. The open symbols are $r_0^{\gamma/1.73}$ computed using the redshift bins listed in Table 2 for the appropriate SED class; these are the same data as shown in Figure 4. The filled symbols are $r_0^{\gamma/1.73}$ for the early- and late-type samples, computed using the redshift bins for the combined sample.

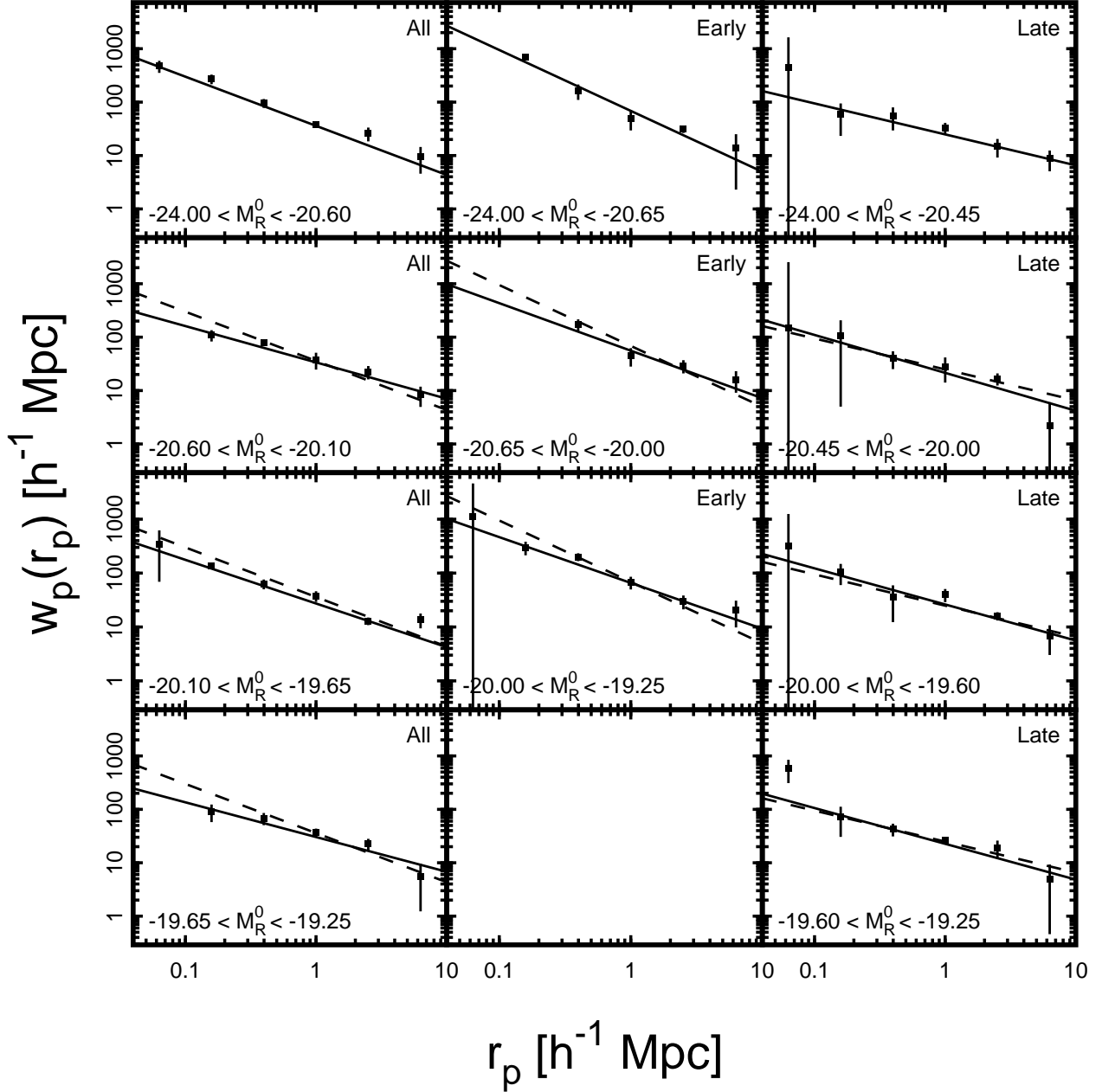


Fig. 10.— Projected comoving correlation function $w_p(r_p)$ for each of the SED- M_R^0 subsamples. The solid line in each panel is the model (equation 2), fit to the data for that subsample; the fit parameters are given in Table 4. The dashed lines show the model from the brightest subsample for each SED class.

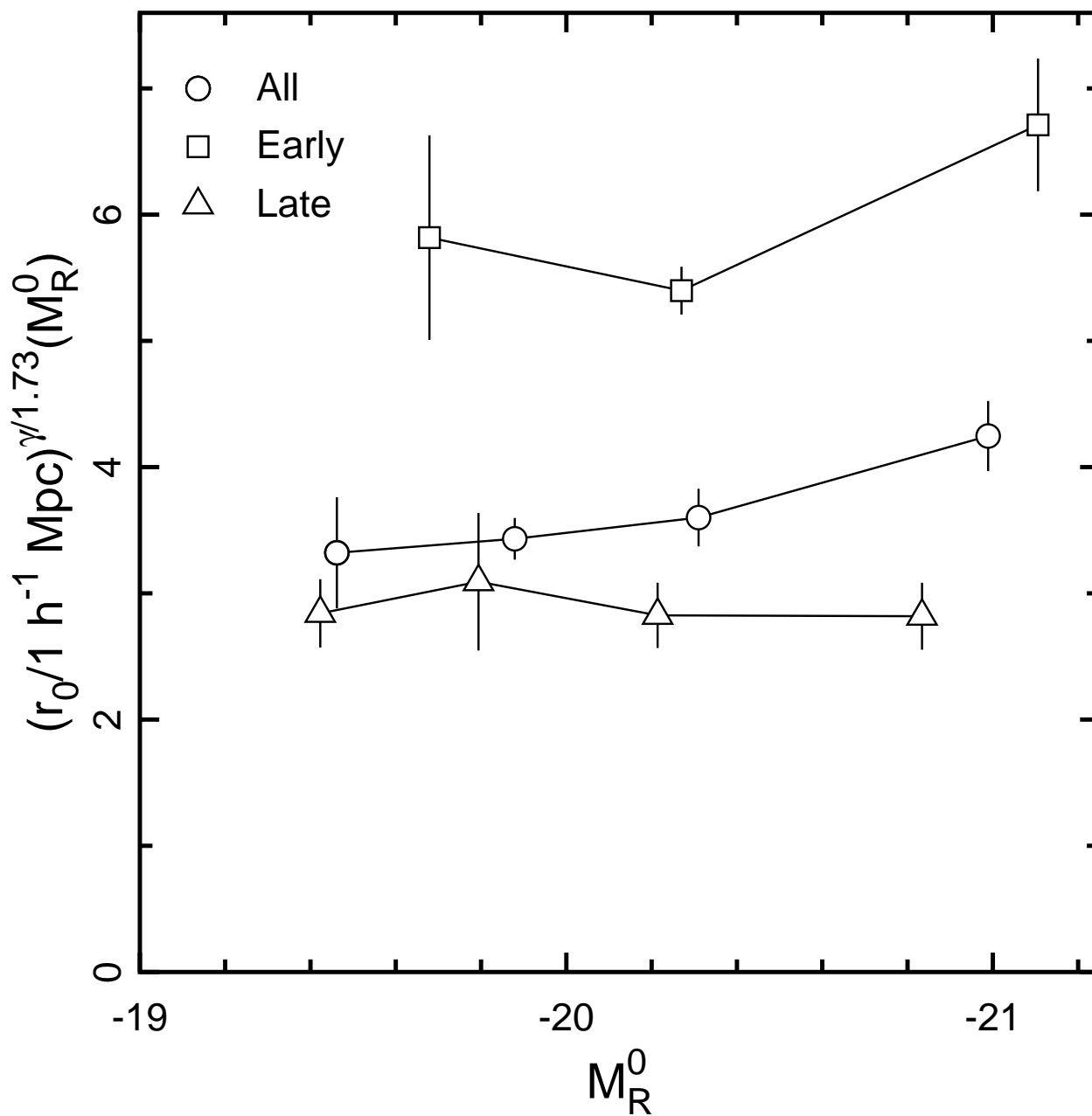


Fig. 11.— Scaled comoving correlation length $r_0^{\gamma/1.73}$ vs. median M_R^0 for each SED- M_R^0 subsample. Each subsample has $0.12 \leq z < 0.40$.

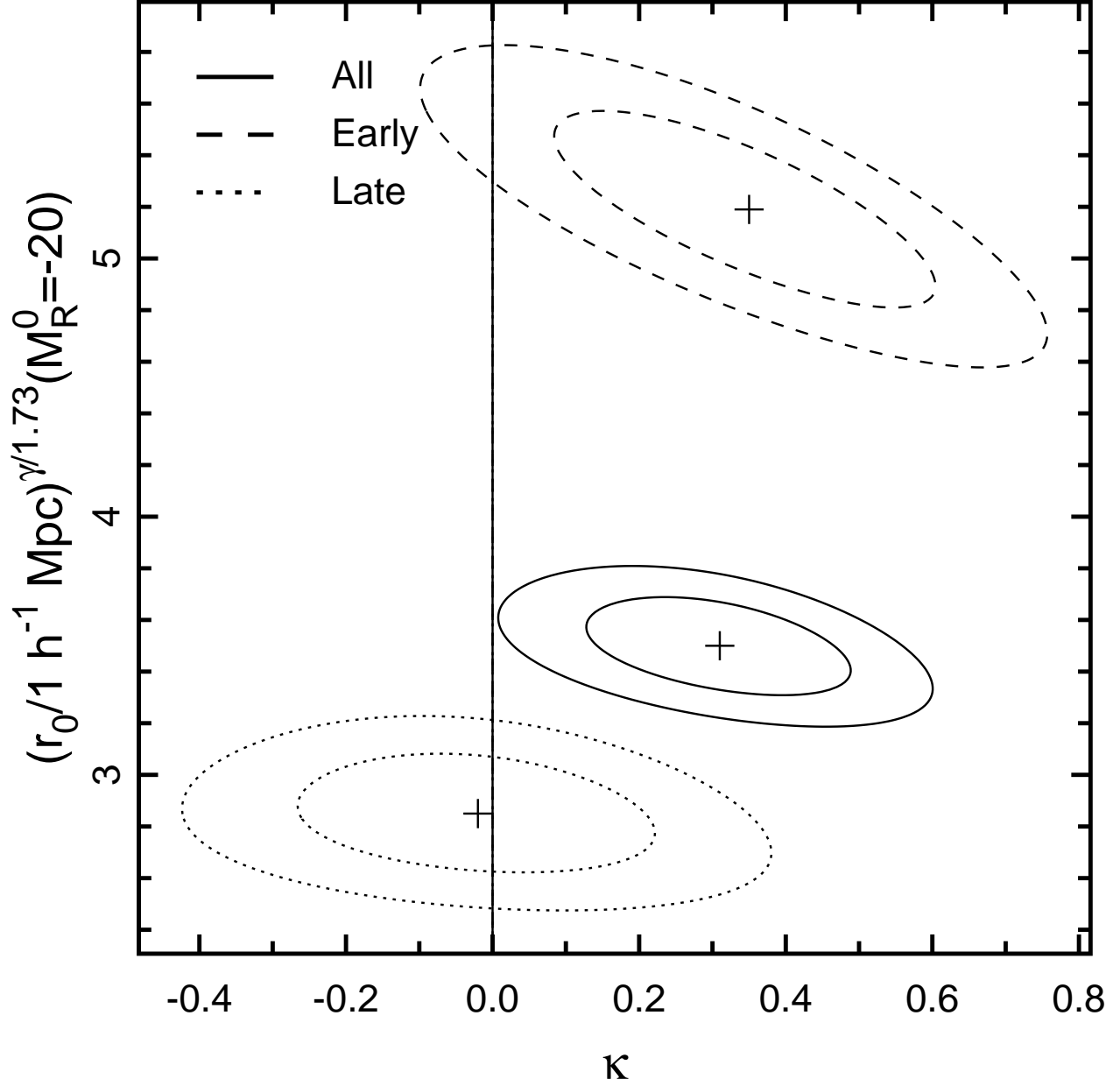


Fig. 12.— One- and 2σ ($\Delta\chi^2 = 2.30$ and 6.17) error contours for the fits of equation (11) for the SED- M_R^0 subsamples.

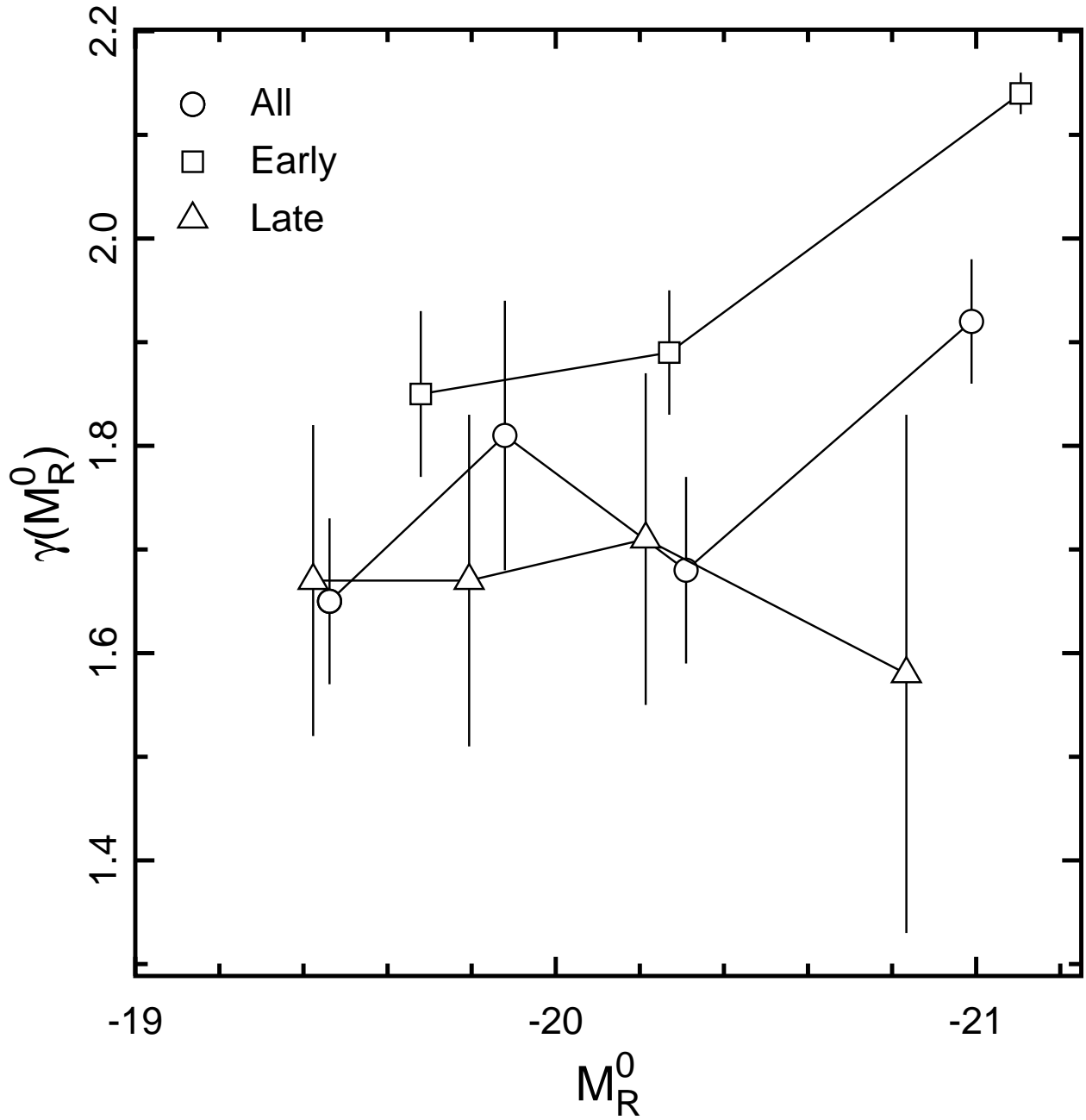


Fig. 13.— Correlation function slope γ vs. median M_R^0 for the SED- M_R^0 subsamples.

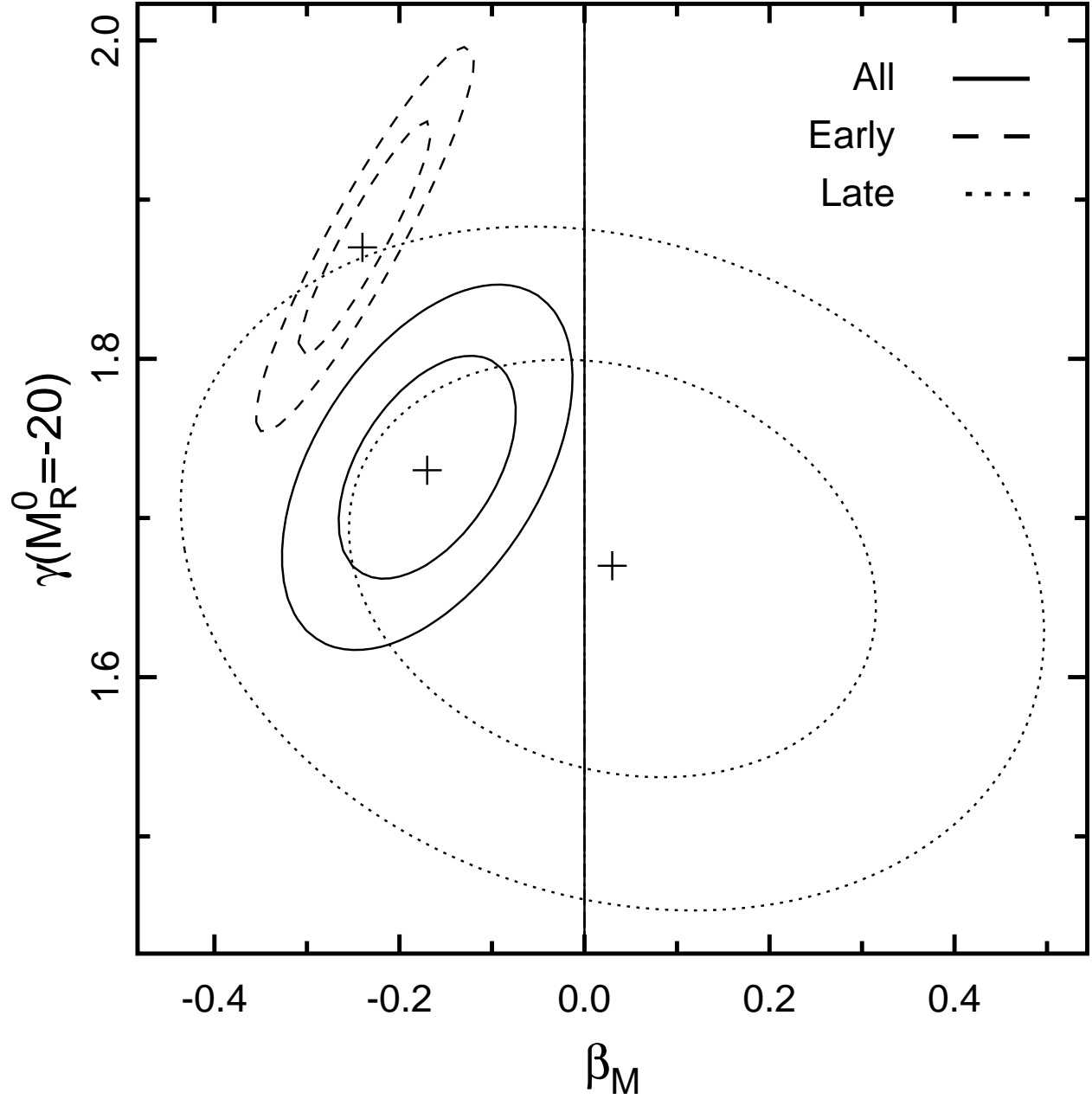


Fig. 14.— One- and 2σ ($\Delta\chi^2 = 2.30$ and 6.17) error contours for the fits of equation (12) for the SED- M_R^0 subsamples.